Origin and Evolution History of Magmatic Garnet-Bearing Pegmatites and Associated Granitoids, Abu Had Area, South Eastern Desert, Egypt: Inference From Petrology and Geochemistry.

Moustafa Esmail Gharib

Geology Department, Faculty of Science, Helwan University
gharibme@yahoo.com

Abstract: Garnet is an uncommon accessory mineral in igneous rocks but is petrologically significant. Pegmatite hosted garnet in Abu Had area is a zoned type and concentration of garnet increase toward the core zone. They intruded the gneissose tonalite-granodiorite and metagabbro country rocks parallel to the Wadi El Gemal major thrust. Isolated large elongated masses or dyke-like bodies of leucogranite intrude the older gneissose tonalite-granodiorite and the metagabbro country rocks along the major thrust fault of Wadi El Gemal in NW-SE direction. The garnets of Abu Had pegmatite have frequently euhedral shape. They are spessartine-almandine rich type displaying reversal zoning with almandine-rich cores and spessartine-rich rims and plotted in the field of magmatic garnet derived from peraluminous S-type granites. Chondrite-normalized REE patterns display a strong enrichment of HREE relative to LREE, and pronounced negative Eu anomalies characteristic features of spessartine-rich garnets crystallized from silicic melts and of garnet in peraluminous granites.
The gneissose tonalite-granodiorite suite has a calc-alkaline metaluminous affinity. It displays the characteristics of I-type granites formed in an island-arc environment and were derived through partial melting of amphibolite source rocks. The leucogranites posses high SiO_2, Al_2O_3 and alkali content, with low TiO_2, MgO, CaO and Fe_2O_3 contents and strongly peraluminous (A=CNK>1.1) characters. They have the geochemical characters of S-type granites and most likely formed in syn-collision regime. Crustal thickening during the collision stage of the Arabian Nubian shiled led to partial- melting of metasedimentary source and other associated crustal rocks along the NW- SE Wadi El Gemal major thrust. Textural features of the studied garnet-bearing pegmatites such as micrographic intergrowth and absence of myrmekite, beside the data of mineral chemistry for the fresh rock-forming minerals support magmatic origin for these pegmatites. Compositional data of primary minerals from the Abu Had pegmatite proved peraluminous source rock magmas. The close spatial distribution of the garnet-bearing pegmatites to the leucogranite country rocks, textural and mineralogical similarity between the leucogranite and the neighboring pegmatites, beside the data of whole rock composition of the leucogranite probably indicate that these rocks are direct precursors to the garnet- bearing pegmatites of Abu Had area. Field and petrographical observations indicate that the garnet-bearing pegmatite affected by post magmatic deformation and metasomatism which often restricted to the microshear zones and fracture sets associated with them. Finally, pinch and swell of the pegmatite dyke, besides cracking and stretching of some garnet crystals in direction perpendicular to the direction of microshear zones, prove that the study pegmatite and the associated country rocks exposed to extension tectonic event post-date the formation of garnet and the associated primary minerals.

[Moustafa Esmail Gharib **Origin and Evolution History of Magmatic Garnet-Bearing Pegmatites and Associated Granitoids, Abu Had Area, South Eastern Desert, Egypt: Inference From Petrology and Geochemistry.**] Journal of American Science 2012;8(10): 536-554]. (ISSN: 1545-1003). http://www.americanscience.org.

Keywords: Magmatic garnet, pegmatite, Abu Had, Wadi El Gemal thrust, Arabian Nubian Shield

1. Introduction

The garnet group of minerals is very widespread and especially characteristic of metamorphic rocks of a wide variety of types, but is not abundant in igneous rocks. Moreover, they are often found in detrital sediments.

Garnet is an uncommon constituent within granite, aplite and pegmatite and has variable compositions and have multifarious origins (Miller & Stoddard 1981; Allan & Clarke 1981; Pattison *et al.*, 1982;; Hamer & Moyes 1982; Kontak and Corey, 1988; Dahlquist *et al.*, 2007, Zhang *et al.*, 2012). Igneous garnet mostly occurs in pegmatites and aplite dykes (Leake, 1967; Manning, 1983; Deer *et al.*,1992; Thöni and Miller, 2004), although its occurrence is also reported in some felsic to very felsic (i.e., SiO_2 ≥70%) peraluminous granitoids (Leake, 1967; Allan and Clarke, 1981; Miller and Stoddard, 1981; du Bray, 1988; Hogan, 1996; Kebede *et al.*, 2001). The vast majority of garnet-bearing granites is S-type and was probably derived from partial melting of predominantly metasedimentary crustal rocks (Chappell and White, 1974; Clemens, 2003). A minority of garnet-bearing granites have more complicated origins than ordinary S-type granites. Some are I-type granites that have undergone unusual fractionation or contamination in volcanic arcs (White *et al.*, 1986; du Bray, 1988; Zhou and Yu, 2001; Wu *et al.*, 2004; Yu *et al.*, 2004), whereas others are A-type granites formed in anorogenic or extensional environments (du Bray, 1988, Zhang *et al*., 2012).

Stone (1988) review the origin of garnet in granitic rocks. Three main modes or mechanism for the origin of garnet in granitic rocks and pegmatites have been proposed; 1) assimilation of pelitic material (Green and Ringwood, 1968; Allan and Clarke, 198l), 2) high pressure phenocrysts or xenocrysts formed at depth and transported to higher levels (Green and Ringwood, 1968; Green, 1977) and 3) crystallisation at low pressure from a peraluminous fluid (Miller and Stoddard, 1981). Chemistry of garnet and the relative proportions of various garnet endmembers can give an idea about possible origin of granitic or pegmatitic magmas and also the approximate depth of formation (Stone, 1988; Harrison, 1988; whitworth, 1992). du Bray (1988) notes that "correlations between garnet composition, host granitoid composition and tectonic setting suggest that garnet chemistry can be employed as an indicator of the tectonic regime prevailing at the time of host granitoid genesis". In general, almandine-rich garnets are associated with less well-evolved granitic rocks, possibly generated at greater depths than more evolved granites which contain high-spessartine garnets.

This study documents the occurrence, distribution, chemistry of garnet and associated minerals hosted by pegmatites from the Abu Had area, south Eastern Desert, Egypt (Figure 1) to employ as indicators for petrogenesis of these rocks. The study also aims to shed light on the relation between the studied pegmatites and granitoid country rocks, beside the link between origins of these rocks with the tectonic evolution of the Arabian Nubian Shield.

2. Regional Geology

The Eastern Desert of Egypt constitutes the northwestern part of the Neoproterozoic Arabian–Nubian Shield (ANS). It constitutes the northern extension of the East African Orogen (EAO) and exposed as a result of uplift prior to opening of the Red Sea (Stern, 1994). It characterized by four main rock sequences: (i) an island arc assemblage; (ii) an ophiolite assemblage; (iii) a gneiss assemblage that comprises the core complexes; and (iv) granitoid intrusions (Abd El-Naby *et al.*, 2000; Abd El-Naby and Frisch, 2002). Hafafit is one of the famous core complexes in the Nubian Shield and represents one of the important suture zones in the Eastern Desert of Egypt. These core complexes have been linked to possible subduction and collision phases during the Neoproterozoic Pan-African orogeny (Stoeser and Camp, 1985; Abdelsalam and Stern, 1993).

El Ramly *et al.* (1994) studied the tectonic evolution of Wadi Hafafit area and environs and called it wadi Hafafit culmination (WHC). This culmination consists of five granitoid-

cored domes composed of medium grade gneisses, separated from the overlying low grade metamorphic rocks by low angle thrust zones (Figure 1). The overlying unit (Nugrus unit) is composed mainly of low grade micaschists and metavolcanics that outcrop in the eastern and northern part of the WHC. These rocks are associated with serpentinites and metagabbros. The underlying unit (Hafafit unit) is represented mainly by the Hafafit domes and consists of (from core to rim): granitic gneiss of tonalitic and trondhjemitic composition, metagabbro and banded amphibolite, altered ultramafic rocks, biotite- and hornblende-gneiss and psammitic gneiss at the rim of the domal structure. Both units have been intruded by leucogranites, especially along thrust zones.

The granitic gneisses in the core of the WHC were earlier regarded as pre-Pan-African basement because of their complex metamorphic and structural history (El Gaby *et al.,* 1988). However, Stern and Hedge (1985) obtained U-Pb dates on zircon of 682 Ma for the granitic core that intrudes the Hafafit gneisses, which they interpreted as being of crystallization age. The latest Pan-African activity in the mapped area (Figure1) is represented by a suite of leucogranites and minor intrusions of pegmatite which intruded the Hafafit gneisses and the ophiolitic assemblage (El Ramly *et al.,* 1993). Elongated narrow intrusive leucogranite is found parallel to the Nugrus thrust (Figure 1a). Several small mnasses and dyke-like plutonic intrusion of leucogranites are found also parallel to Wadi El Gemal thrust beside the large leucogranite pluton forming Gabal El Falig (Figure 1b). Generally, these leucogranites are garnet-bearing, e.g. garnetiferous granites.

Abd El-Naby *et al.,* 2008 stated that WHC was affected by two main metamorphic phases. The first metamorphic phase (M1), observed in the micaschists of the Nugrus unit, is characterized by greenschist-facies conditions, yield temperatures of 400°–550°C and reveals pressure of 3.7-4.9 kbar. The second metamorphic phase (M2), observed in gneisses and amphibolites of the Hafafit unit, is characterized by amphibolite-facies conditions, yield temperatures of 600°–750°C and pressures of 6-8 kbar. They recorded Sm-Nd and Rb-Sr whole rock-mineral isochron ages around 590 Ma for these gneisses and amphibolites and stated that this age probably represent cooling from the metamorphic thermal peak which was attained around 600 Ma or slightly earlier. This geochronological data is in accordance with the emplacement ages of the leucogranites from two different localities in Sikait area along major Nugrus thrust (about 20km north east of the studied area) ranges between 610±20 and 594± 12Ma and interpreted as emplacement ages for these granites (Moghazi *et al.,* 2004). Because of the similarity between the dates of metamorphism and granite emplacement in Hafafit-Nugrus area, they propose that both of metamorphic rocks and leucogranites are the products of the same event that occurred during collision and thrusting stage. On the other hand, Fritz *et al.* (2002) reported $^{40}Ar/^{39}Ar$ ages of 586 Ma for hornblende separated from the granitic core of the Hafafit domes. They interpreted these ages as cooling ages below 500°C associated with exhumation of WHC along localized NE-trending extensional faults.

2.1. Local geology

Abu Had area lies to the south of the Migif-Hafafit metamorphic core complex along Wadi Hafafit-Wadi El Gemal road. The main rock units encountered in this area are from older to younger include; metagabbros, gneissose tonalite-ganodioite, leucoganites and pegmatite (Figure 1b).

The metagabbro country rocks are medium to coarse-grained, intensely deformed and well foliated. The contact between the metagabbro and the intruded gneissic tonalite-granodiorite is generally sharp.

The gneissic tonalite-granodiorite is medium to coarse-grained greyish to greyish green in colour and show distinct foliation. Bouldery wreathing and exfoliation are well exhibited. Contact between gneissic granite and the intruded pegmatites are sharp with small thermal effect toward the intruded granitoids.

Isolated large elongated masses or dike-like bodies of leucogranite intrude the older gneissose tonalite-granodiorite and the metagabbro country rocks mainly in the east side of Abu Had area and ending with the largest elongated shape leucogranite of Gabal El Falig to the west of the area (Figure 1b). The leucogranites are characterized by white to whitish grey colour, fine to coarse-grained and occasionally pegmatitic. Generally, these rocks are garnet-bearing and developed along the major thrust fault of Wadi El Gemal in NW-SE direction. On the other hand, a NNW-SSE strike-slip faults most probably relate to the Najd fault system dislocates the leucogranites pluton with common displacement and some parts of the leucogranite affected by shearing stress.

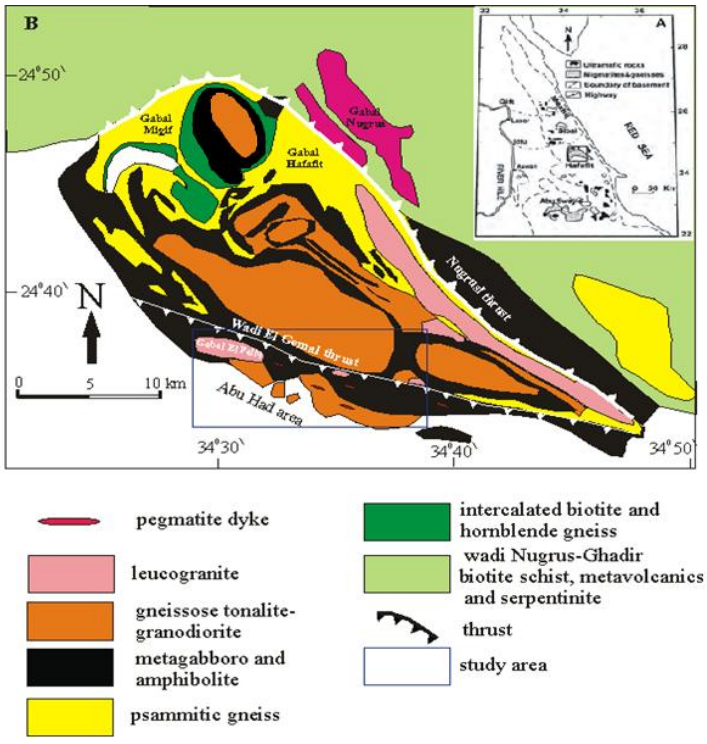

Figure 1. A) Location map of the study area. B) General geological map of the study area (modified from El Ramly et al., 1993).

Pegmatites in Abu Had area occur as dykes extend for more than 1 kilometres, varying in width reach more than 20m, internally zoned and mainly have NW-SE direction. These dykes are garnet-bearing and shows pinch and swell structure and dominated by vertical joints (Figures 2a and b). They intrude the gneissose granitoids and metagabbro country rocks parallel to the major thrust of Wadi El Gemal. Contacts between pegmatite and the intruded rocks are generally sharp. Internal zoning of Abu Had pegmatites consists of outer zones concentric upon a core (Figure 2c).The outer border zone is more fine grained relative the inner zones and contain abundant muscovite, while the intermediate and core zones are highly enriched in garnet. Shearing stress and microfracture are well observed in the extremely coarse-grained inner zones (Figures 2d and e).

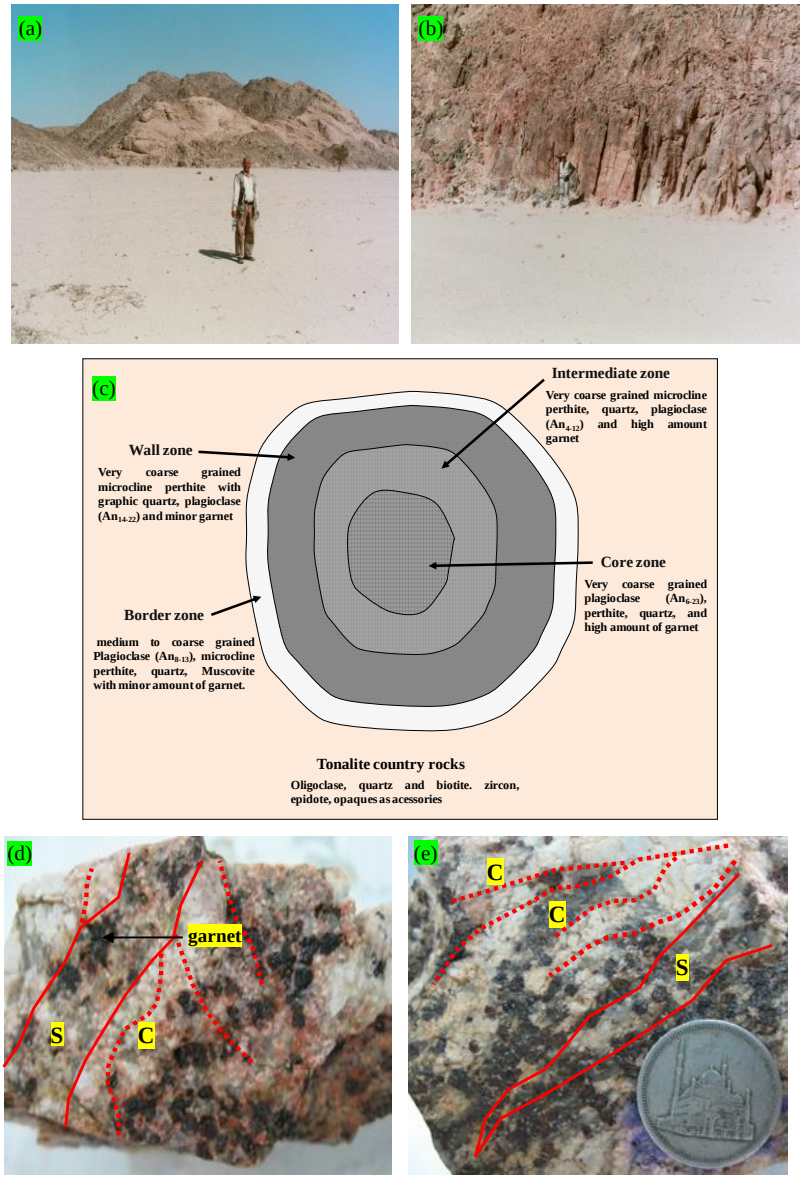

Fig.2. Field photo showing (a) pinch and swell in the garnet- bearing pegmatite dyke which cut the gneissose granodiorite-tonalite. (b) abundant of vertical joints in pegmatite dyke. (c) schematic cross section across Abu Had garnet-bearing pegmatite which intruded the gneissose tonalite- granodiorite showing zonal structure. (d) handspecimen from intermediate zone of garnet- bearing pegmatite showing abundant of garnet and show minor shear zone (S). (e) handspecimen from core zone showing abundant of garnet and show minor shear zone (S) and cleavage (C).

3. Petrography

The metagabbro country rocks are medium to coarse-grained dark green rocks and highly foliated. It is composed mainly of plagioclase, hornblende and clinopyroxene. Quartz, opaque and sphene are accessories. Clinopyroxene is mainly altered to tremolite and saussurite. Hornblende is occurs as suhedral green crystals, some are chloritized and contain inclusions of apatite and opaque minerals. Some hornblende contains inclusions of plagioclase and quartz. Plagioclase occurs as anhedral crystal highly deformed mainly with distinct lamellar twinning and sometimes shows zoning. It ranges in composition from andesine to labradorite (An_{30-57}). Quartz occurs as irregular interstitial grains corroding plagioclase and hornblende.

Gneissose granodiorite-tonalite is medium to coarse-grained rocks, show gneissose texture and moderately deform. They are composed essentially of plagioclase, quartz, biotite and minor orthoclase in decreasing order of abundance. Accessory minerals include opaque minerals, apatite and sphene. The rocks show a gneissic texture where biotite is oriented in parallel alignment. Plagioclase represents essentially by oligoclase and range in composition from $An_{(12-20)}$ and mainly shows albite twinning. Biotite occurs as medium to coarse brown flakes characterized by strong pleochroism. It sometimes encloses minute apatite inclusions. Some biotite altered to chlorite.

Orthoclase occurs as anhedral crystal rarely showing graphic and perthitic textures.

The Leucogranite rocks are slightly deformed and in some parts suffered fracture and shearing stress. They are consisting mainly of quartz, plagioclase and K-feldspar with small amounts of biotite, muscovite and garnet. Zircon, opaque and monazite are the main accessories. Plagioclase (An_{15-26}) occurs as subhedral crysrtals and generally shows albite twinning. Potash feldspar represented mainly by microcline and microcline perthite. Garnet occurs as equigranular euhedral to suhedral grains and show equilibrium boundaries with both quartz and feldspar (Figure 3a). High magnification for zircon crystal from the leucogranite (Figure 3b) proved their relation to S-type granites (granites of crustal origin) according to the typological classification of zircon (Pupin, 1980).

Petrographical study of the internal zoning of the garnet bearing pegmatite indicates heterogeneous composition from the border zone inward to the core. The border zone consists predominantly of medium to coarse-grained plagioclase (An_{8-12}), microcline perthite, quartz, muscovite with minor garnet. Zircon occurs as accessory and mainly associated or as inclusion in garnet (Figures 3c and d). Muscovite occur as coarse flakes characterized by colourless to pale green colour with distinct cleavage (Figure 3d). The wall zone composed of very coarse grained microcline perthite with graphic quartz, plagioclase (An_{15-23}) and minor garnet. The intermediate zone comprises very coarse grained crystals of microcline perthite, quartz, plagioclase (An_{3-16}) and high amount of garnet (Figure 3e). The core zone represents by very coarse grained plagioclase (An_{6-23}), perthite, quartz with high enrichment in garnet crystal. Garnet represents more than 30% by volume for the core zone. Some of the course grain garnet crystals contain inclusions of zoned allanite which sometime include inclusion of epidote (Figures 3f and g), proved their magmatic origin.

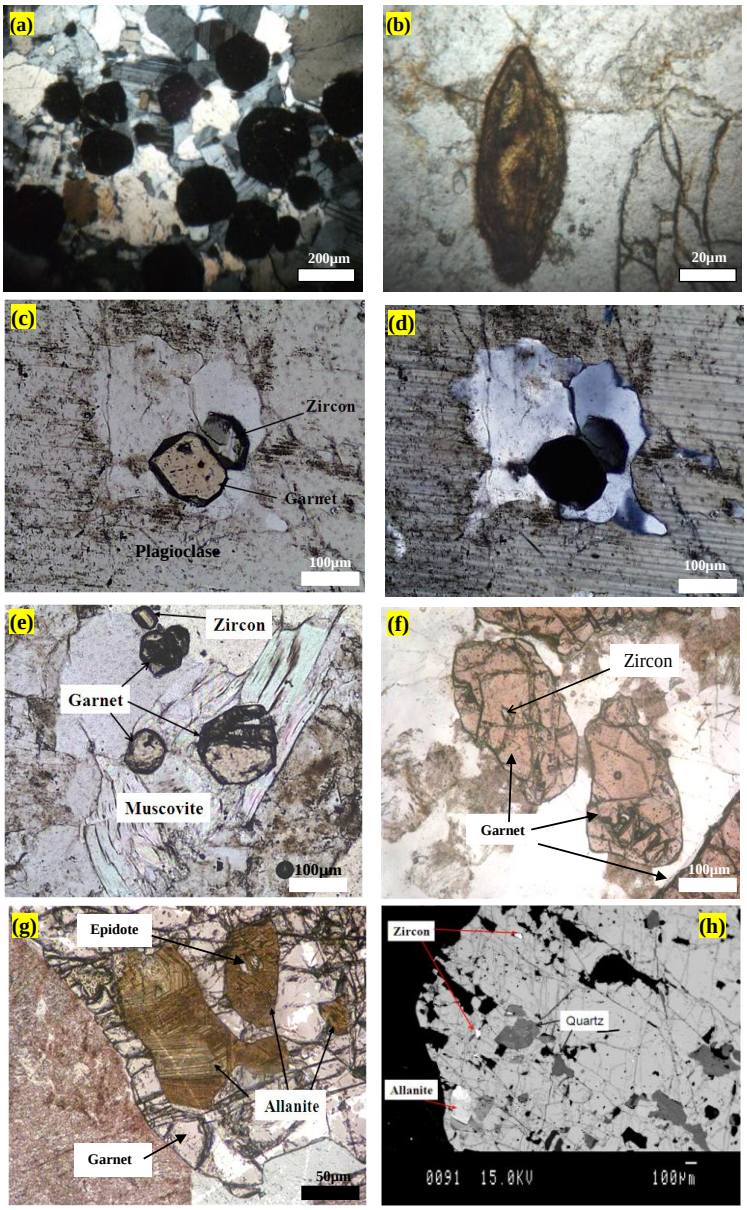

Fig.3. Photomicrograph showing (a) leucogranite with abundant euhedral to subhedral garnet crystals (Black colour). (b) Euhedral metamict zircon crystal in leucogranite. (c -d) euhedral garnet and zircon crystals associated quartz and plagioclase in wall zone of garnet-bearing pegmatite. (e) garnet, zircon and muscovite in border zone of garnet-bearing pegmatite. (f) coarse-grained garnet in the intermediate zone of pegmatite. (g) zoned allanite with inclusion of epidote within garnet crystals from the pegmatite core zone. (g) Back-scattered electron (BSE) image showing zoned allanite and zircon as inclusion within garnet crystal**.**

Generally, textures in Abu Had leucogranites and garnet-bearing pegmatites are dominated by magmatic features. The coarse-grained magmatic assemblages were affected to some extent by post magmatic deformation which confined to mm-scale microstructure shears zones or bands (S) and cleavage or fracture planes (C). Features of post-magmatic deformation include; 1) undulose extinction of quartz and abundant of secondary quartz in shear bands (Figures 4a,b and c). 2) tilting and stretching of the muscovite flakes (Figure 4d). 3) gliding in the of albite twinning in plagioclase (Figure 4e) and transformation of some plagioclase to secondary albite and sericite. 4) breakdown of some garnet to chlorite and iron oxide in the microshear bands along garnet peripheries and the interstitial fractures (Figure 4f). 5) tilting and stetching of some garnet crystals in the shear bands perpendicular to the shear zone (Figures 4g,h). 5) presence of fine grained muscovite or sericite along microcracks or cleavage plains. All these features post-date the garnet and primary minerals formation.

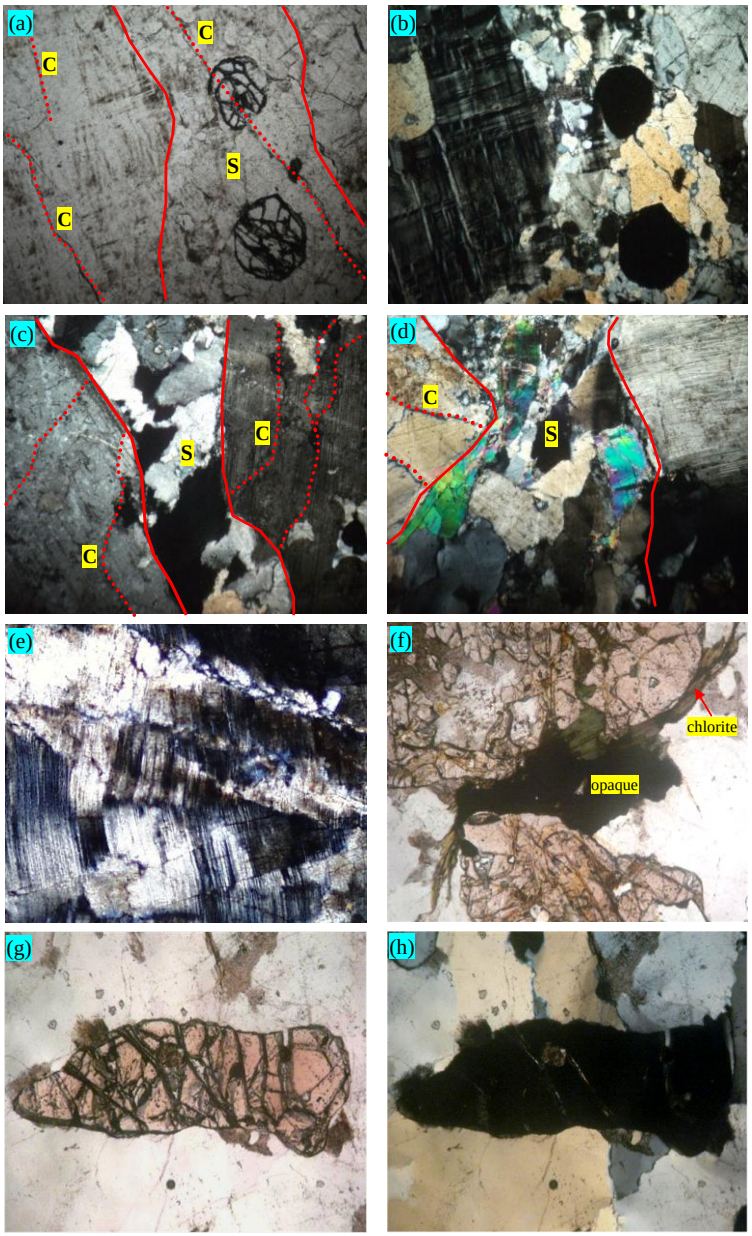

Fig.4. Photomicrograph showing (a -b) microshear zone (S) and cleavage (S) in leucogranite. (c) shear zone and cleavage in wall zone of garnet-bearing pegmatite. (d) microshear zone in the intermediate zone of garnet-bearing pegmatite. (e) gliding of albite twinning in plagioclase of the core zone. (f) breakdown of garnet to chlorite and opaque in shear zone within the pegmatite. (g-h) stretching and fracturing of garnet crystal in direction perpendicular to the microshear zone in the pegmatite core zone.

4. Analytical methods

In-situ analyses of silicate minerals including feldspars, muscovite, garnet and chlorite from Abu Had pegmatites were carried out using a JEOL probe JXA-800 at the Institute of Mineralogy, Salzburg University, Austria. Analytical conditions were 15 kV accelerating voltage, 20 nA probe current and 3 µm beam diameter using various natural and synthetic standards. The raw data were corrected with an on-line ZAF program. Major element X-ray mapping of garnet from the studied pegmatite was made after the electron microprobe (EMP) analyses in order to check whether the spots were representative of the chemical zoning or not.

In-situ trace and REE analysis for garnet crystals from Abu Had pegmatite were determined by laser-ablation (193 nm ArF excimer: MicroLas GeoLas Q-plus)-inductively coupled plasma mass spectrometry (Agilent 7500S) (LA-ICP-MS) at

Kanazawa University, Japan. Analyses were performed by ablating 60-μm diameter spots. All analyses were performed at 6 Hz with energy density of 8 J/cm^2 per pulse. Details of the analytical procedures have been described by Ishida *et al.* (2004) and Morishita *et al*. (2005). Calibration of LA-ICP-MS analysis was carried out by using external standard as NIST 610, assuming the composition given by Pearce *et al.* (1997). Precision or reproducibility is better than 6% for most elements, except B, Nb, and Ta which it is better than 11-13%.

Representative samples from the granitoids country rocks for the garnet-bearing pegmatite
dykes, including gneissose granitoids (7 samples), and leucogranite (5 samples) have been analyzed for major and trace element composition, and some further selected samples were analyzed for rare-earth elements (REE). Each analysis was performed on a 0.2 g sample by inductively coupled plasma-mass spectrometry (ICP-MS) following a LiBO2 fusion and dilute nitric acid digestion. All whole rock analyses were carried out in ACME analytical laboratories (Canada).

5. Mineral chemistry

5.1. Feldspar

Representative analyses of feldspars and their calculated formulae are given in Tables 1&2.

The plagioclase composition from Abu Had pegmatite is dominated by albite-oligoclase composition (An_{8-23}) with decreasing Ca-content towards the rim. Few subgrains in the matrix are more albite-rich (an_{2-6}). The Or component is generally less than 3% (Table 1).

The alkali feldspar from the different pegmatite zones represent mainly by coarse grained microcline perthite. Microprobe analyses of K-feldspar (Table 2) indicate compositions of Or_{88-98} Ab_{2-13} $An_{0-0.34}$.The bulk composition of K-feldspar shows minor variations in Na and Ca across the different pegmatite zones. The Na_2O contents vary from 0.19 to 1.48 wt.%, whereas uniformly low levels of CaO (0.00–0.07 wt.%) are typical of all the studied pegmatites.

Table 1. Representative major oxide composition of plagioclase from different pegmatite zones, Abu Had Area, Eastern Desert, Egypt.

Element	Plagioclase Core zone				Plagioclase Intermediate zone					Plagioclase Wall zone					Plagioclase Border zone	
	core	rim	matrix	core	core	rim	matrix	matrix	matrix	core	rim	core	core	rim	core	rim
SiO_2	63.00	63.60	66.07	63.80	64.00	65.40	68.56	65.80	66.90	62.50	62.00	62.90	63.00	62.30	65.40	66.00
TiO_2	0.00	0.02	0.00	0.01	0.00	0.00	0.00	0.00	0.03	0.00	0.00	0.00	0.00	0.00	0.00	0.00
Al_2O_3	23.70	23.10	21.10	23.49	22.9	22.40	20.47	22.60	22.12	23.70	23.90	23.40	23.30	24.00	21.90	21.10
FeO	0.09	0.30	0.02	0.08	0.00	0.05	0.18	0.05	0.00	0.10	0.10	0.06	0.00	0.10	0.00	0.12
MnO	0.00	0.10	0.01	0.00	0.00	0.00	0.11	0.00	0.01	0.00	0.00	0.00	0.00	0.00	0.00	0.08
MgO	0.00	0.05	0.00	0.00	0.02	0.09	0.02	0.09	0.03	0.00	0.00	0.00	0.00	0.02	0.00	0.00
CaO	4.60	3.55	1.47	4.25	3.4	1.88	0.50	0.68	0.51	4.59	5.00	4.10	4.30	3.10	2.52	1.72
Na_2O	8.50	8.90	11.52	8.40	9.5	10.28	10.62	10.28	10.25	8.90	8.70	9.20	9.10	9.10	10.00	10.60
K_2O	0.17	0.40	0.15	0.21	0.12	0.33	0.02	0.49	0.23	0.15	0.40	0.31	0.25	1.10	0.14	0.18
Total	100.07	100.03	100.33	100.23	99.94	100.43	100.49	100.01	100.10	99.94	100.10	99.97	99.95	99.72	99.96	99.80
Chemical formula based on 8 (O)																
Si	2.78	2.81	2.90	2.80	2.82	2.86	2.97	2.88	2.91	2.77	2.75	2.78	2.79	2.77	2.87	2.91
Ti	0.00	0.00	0.00	0.00	0.00	0.00	0.00	0.00	0.00	0.00	0.00	0.00	0.00	0.00	0.00	0.00
Al	1.23	1.20	1.09	1.22	1.19	1.16	1.05	1.17	1.14	1.24	1.25	1.22	1.22	1.26	1.13	1.09
Cr	0.00	0.00	0.00	0.00	0.00	0.00	0.00	0.00	0.00	0.00	0.00	0.00	0.00	0.00	0.00	0.00
Fe	0.00	0.01	0.00	0.00	0.00	0.01	0.01	0.00	0.00	0.00	0.00	0.00	0.00	0.00	0.00	0.00
Mn	0.00	0.00	0.00	0.00	0.00	0.00	0.00	0.00	0.00	0.00	0.00	0.00	0.00	0.00	0.00	0.00
Mg	0.00	0.00	0.00	0.00	0.01	0.01	0.00	0.01	0.00	0.00	0.00	0.00	0.00	0.00	0.00	0.00
Ca	0.22	0.17	0.07	0.20	0.16	0.09	0.02	0.03	0.02	0.22	0.24	0.19	0.20	0.15	0.12	0.08
Na	0.73	0.76	0.98	0.72	0.81	0.87	0.89	0.87	0.86	0.76	0.75	0.79	0.78	0.78	0.85	0.90
K	0.01	0.02	0.01	0.01	0.01	0.02	0.00	0.03	0.01	0.01	0.02	0.02	0.01	0.06	0.01	0.01
Total	4.97	4.98	5.05	4.95	4.99	5.00	4.95	4.99	4.96	5.00	5.01	5.01	5.00	5.03	4.99	5.00
An	22.79	17.63	6.54	21.58	16.40	9.01	2.52	3.42	2.66	21.99	23.57	19.42	20.42	14.85	12.13	8.15
Ab	76.20	79.98	92.65	77.16	82.91	89.11	97.38	93.67	95.94	77.15	74.19	78.83	78.17	78.88	87.07	90.84
Or	1.00	2.38	0.81	1.27	0.69	1.88	0.10	2.91	1.40	0.86	2.24	1.75	1.41	6.27	0.80	1.02

5. 2. Muscovite

The white micas in the studied pegmatite occur in two forms; primary muscovite which occurs as euhedral to subhedral coarse-grained flakes and show sharp contact with the associated primary minerals such as feldspar, quartz and garnet, and secondary muscovite grains have resulted from post magmatic or shear deformation. They appear as medium to coarse-grained highly deformed flakes or as fine-grained intestinal aggregates. White mica was taken to determine whether it is of primary or secondary origin, since primary white mica is widely held to be an indicator of peraluminous magmas (Speer, 1984). Selected muscovite analyses from Abu Had pegmatite and their structural formulae are given in Table 3. Plotting data of the studied muscovite on the triangular diagram Mg-Ti-Na diagram adopted by Miller *et al.*(1981) revealed presence of primary and secondary muscovite. The large muscovite grains have a high TiO_2 content and consistently fall in the primary muscovite field in the Mg–Ti–Na ternary diagram (Miller *et al.*, 1981), while the deformed and interstitial flakes from the shear zones plot in the secondary muscovite field (Figure 5).

Primary magmatic muscovite has also distinctive composition similar to those in typical S-type granitoids (Figure 5). According to Monier *et al.* (1984), the ratio of Na/ (Na+K) is also a good indicator for distinguishing the origin of muscovite (primary: Na/(Na+K) = 0.06–0.12; post-and late-magmatic: 0.01–0.07; hydrothermal: < 0.04). In the case of the Abu Had pegmatite, primary muscovite has a higher Na/(Na+K) ratio >0.06 compared to secondary muscovite <0.06 (Table 3).

Generally, the analyzed muscovite from the border and wall pegmatite zones related to the primary magmatic muscovite, while deformed and aggregates muscovite selected from the shear zones in the intermediate and core zones related to post magmatic and hydrothermal muscovite. Thus, both petrographical and chemical evidence indicate a primary origin for some muscovite of the Abu Had pegmatite.

5.3. Garnet

Some coarse-grained, fresh euhedral to subhedral garnet crystals were selected for EMP analyses (Table 4). The analyzed coarse-grained garnets are essentially almandine–spessartine solid solutions, characteristic for magmatic pegmatite garnet

(Whitworth and Feely, 1994). In all samples these two end-members in the range 76.51-96.25 mol% of the garnet, pyrope range from 1.45-9.35 mol%, grossular varied between 1.23-22.4 mol%. Generally, spessartine contents decrease within the pegmatite zones from 54.1 mol% on an average in the border zone to 34.51mol% on an average in the pegmatite core zone. In contrast, reverse relation was documented for grossular which range from 1.3mol% an average in the border zone to 18.01mol% on an average in the pegmatite core zone, while pyrobe and almandine showed variable contents within the pegmatite zones (Table 4). The spessartine component is significant in all analyses of garnet, consistent with the findings of previous studies of garnets from peraluminous granitoids. With reference to the fields outlined by Miller & Stoddard (1981) for plutonic garnet (Figure 6), the studied garnet compositions conform to those considered indicative of magmatic conditions and, in particular similar to garnet from peraluminous granitoids reported by du Bray, 1988 and Dahlquist *et al.*, 2007 with somewhat enrichment in Mn content.

Table 2. Representative major oxides of K-feldspar from different pegmatite zones, Abu Had area, South Eastern Desert, Egypt.

Sammple No.	K-feldspar		K-feldspar			K-feldpar								K-feldspar						
Element	Core zone		Intermediate zone			Wall zone								Border zone						
SiO_2	65.30	65.50	65.88	66.40	66.00	64.60	64.40	64.90	64.00	64.80	65.30	64.30	64.60	64.70	64.60	65.00	64.40	64.00	64.20	64.00
TiO_2	0.01	0.01	0.05	0.00	0.03	0.01	0.00	0.00	0.00	0.00	0.00	0.00	0.00	0.00	0.00	0.00	0.00	0.00	0.00	0.00
Al_2O_3	18.80	18.40	19.00	19.00	18.90	18.70	18.70	18.60	18.80	18.80	18.70	18.70	18.60	18.60	18.75	18.60	18.60	18.50	18.50	18.48
FeO	0.00	0.06	0.16	0.25	0.06	0.00	0.00	0.00	0.00	0.00	0.00	0.12	0.00	0.00	0.00	0.00	0.00	0.00	0.00	0.00
MnO	0.00	0.00	0.00	0.01	0.00	0.00	0.00	0.00	0.00	0.00	0.00	0.08	0.00	0.00	0.00	0.00	0.00	0.00	0.00	0.00
MgO	0.00	0.00	0.02	0.06	0.00	0.00	0.00	0.00	0.00	0.00	0.00	0.00	0.00	0.00	0.02	0.00	0.00	0.00	0.00	0.00
CaO	0.02	0.04	0.01	0.01	0.00	0.00	0.06	0.05	0.05	0.07	0.00	0.00	0.00	0.00	0.00	0.00	0.00	0.00	0.00	0.00
Na_2O	0.86	0.83	0.23	0.40	0.19	1.48	0.75	1.37	0.78	1.28	0.44	0.38	0.97	0.47	0.65	0.44	0.36	0.68	0.54	0.60
K_2O	14.90	15.30	15.60	14.00	14.50	15.00	16.10	15.00	16.00	15.10	16.10	16.43	15.60	16.50	16.00	16.05	16.60	16.40	16.20	16.26
Total	99.90	100.14	100.95	100.13	99.69	99.79	100.01	99.92	99.63	100.05	100.54	100.01	99.77	100.27	100.02	100.09	99.96	99.58	99.44	99.34
Chemical formula based on 8 (O)																				
Si	3.00	3.01	3.00	3.02	3.02	2.98	2.98	2.99	2.97	2.98	3.00	2.98	2.99	2.99	2.98	3.00	2.98	2.98	2.99	2.98
Ti	0.00	0.00	0.00	0.00	0.00	0.00	0.00	0.00	0.00	0.00	0.00	0.00	0.00	0.00	0.00	0.00	0.00	0.00	0.00	0.00
Al	1.02	1.00	1.02	1.02	1.02	1.02	1.02	1.01	1.03	1.02	1.01	1.02	1.01	1.01	1.02	1.01	1.02	1.02	1.01	1.02
Cr	0.00	0.00	0.00	0.00	0.00	0.00	0.00	0.00	0.00	0.00	0.00	0.00	0.00	0.00	0.00	0.00	0.00	0.00	0.00	0.00
Fe	0.00	0.00	0.01	0.01	0.00	0.00	0.00	0.00	0.00	0.00	0.00	0.00	0.00	0.00	0.00	0.00	0.00	0.00	0.00	0.00
Mn	0.00	0.00	0.00	0.00	0.00	0.00	0.00	0.00	0.00	0.00	0.00	0.00	0.00	0.00	0.00	0.00	0.00	0.00	0.00	0.00
Mg	0.00	0.00	0.00	0.00	0.00	0.00	0.00	0.00	0.00	0.00	0.00	0.00	0.00	0.00	0.00	0.00	0.00	0.00	0.00	0.00
Ca	0.00	0.00	0.00	0.00	0.00	0.00	0.00	0.00	0.00	0.00	0.00	0.00	0.00	0.00	0.00	0.00	0.00	0.00	0.00	0.00
Na	0.08	0.07	0.02	0.04	0.02	0.13	0.07	0.12	0.07	0.11	0.04	0.03	0.09	0.04	0.06	0.04	0.03	0.06	0.05	0.05
K	0.87	0.90	0.91	0.81	0.85	0.88	0.95	0.88	0.95	0.89	0.94	0.97	0.92	0.97	0.94	0.94	0.98	0.97	0.96	0.97
Sum	4.97	4.98	4.95	4.90	4.90	5.02	5.02	5.01	5.02	5.01	4.99	5.01	5.01	5.01	5.01	4.99	5.01	5.03	5.01	5.02
An	0.12	0.18	0.06	0.05	0.00	0.00	0.29	0.25	0.24	0.34	0.00	0.00	0.00	0.00	0.00	0.00	0.00	0.00	0.00	0.00
Ab	8.05	7.58	2.22	4.18	1.96	13.04	6.59	12.16	6.88	11.37	3.99	3.40	8.63	4.15	5.81	4.00	3.19	5.93	4.82	5.31
Or	91.82	92.23	97.71	95.77	98.04	86.96	93.12	87.60	92.88	88.28	96.01	96.60	91.37	95.85	94.19	96.00	96.81	94.07	95.18	94.69

Table 3. Representative major oxidescomposition of muscovite in Abu Had garnet-bearing pegmatite,South Eastern Desert, Egypt.

Element	Muscovite Core zone					Muscovite Intermediate zone			Muscovite Wall zone	Muscovite Border zone		
SiO_2	46.51	46.02	46.60	47.00	49.21	49.50	46.50	48.00	46.00	45.00	45.00	45.80
TiO_2	0.24	0.37	0.32	0.49	0.19	0.17	0.43	0.00	0.80	0.17	0.38	0.40
Al_2O_3	26.17	29.22	29.30	29.20	31.40	29.50	31.20	39.00	33.38	33.80	33.40	34.00
Cr_2O_3	0.00	0.01	0.02	0.00	0.01	0.00	0.00	0.00	0.00	0.00	0.00	0.00
FeO	9.11	6.38	6.85	7.00	5.20	5.80	6.80	0.82	5.00	4.80	3.60	3.70
MnO	0.35	0.13	0.28	0.31	0.10	0.15	0.43	0.10	0.27	0.05	0.00	0.00
MgO	2.21	1.77	1.90	2.50	1.74	3.00	2.30	0.21	0.46	0.16	0.53	0.52
CaO	0.03	0.00	0.12	0.02	0.01	0.09	0.05	0.05	0.00	0.00	0.00	0.00
Na_2O	0.11	0.21	0.20	0.19	0.04	0.18	0.09	0.24	0.53	0.46	0.76	0.72
K_2O	10.75	10.95	9.53	8.00	7.00	6.80	6.90	7.60	9.80	9.90	10.40	10.30
Total	95.48	95.06	95.12	94.70	94.89	95.19	94.71	96.02	96.24	94.34	94.07	95.44
Chemical formula based on 22 (O)												
Si	6.48	6.35	6.38	6.40	6.53	6.58	6.28	6.17	6.17	6.15	6.16	6.16
Al^{4+}	1.52	1.65	1.62	1.60	1.47	1.42	1.72	1.83	1.83	1.85	1.84	1.84
Z	8.00	8.00	8.00	8.00	8.00	8.00	8.00	8.00	8.00	8.00	8.00	8.00
Al^{6+}	2.78	3.10	3.11	3.09	3.44	3.20	3.25	4.08	3.53	3.59	3.54	3.56
Ti	0.02	0.04	0.03	0.05	0.02	0.02	0.04	0.00	0.08	0.02	0.04	0.04
Fe	1.06	0.74	0.78	0.80	0.58	0.64	0.77	0.09	0.57	0.55	0.41	0.42
Mn	0.04	0.02	0.03	0.04	0.01	0.02	0.05	0.01	0.03	0.01	0.00	0.00
Mg	0.46	0.36	0.39	0.51	0.34	0.59	0.46	0.04	0.10	0.03	0.11	0.10
Y	4.37	4.25	4.35	4.48	4.40	4.48	4.58	4.22	4.31	4.19	4.10	4.12
Ca	0.00	0.00	0.02	0.00	0.00	0.01	0.01	0.01	0.00	0.00	0.00	0.00
Na	0.03	0.05	0.05	0.05	0.01	0.05	0.02	0.06	0.14	0.12	0.20	0.19
K	1.91	1.93	1.66	1.39	1.19	1.15	1.19	1.25	1.71	1.72	1.82	1.77
Z	1.95	1.98	1.73	1.44	1.20	1.21	1.22	1.31	1.85	1.85	2.02	1.96
Total	14.32	14.23	14.08	13.92	13.59	13.69	13.80	13.53	14.16	14.04	14.12	14.08
Fe/Feo+MgO	0.70	0.67	0.67	0.61	0.63	0.52	0.62	0.69	0.86	0.94	0.79	0.80
Na/Na+K	0.02	0.03	0.03	0.03	0.01	0.04	0.02	0.05	0.08	0.07	0.10	0.10

Four euhedral garnet crystals from the different pegmatite zones were chosen for composition zoning profiles beside large crystal from the intermediate zone was selected for X-ray composition mapping profile. The results of major element analysis profiles within the garnet crystals from cores to rims from different pegmatite zones
are shown in Figure 7. Data analysis of the studied garnets proved that the rim contains low FeO contents but high MnO contents relative to the cores. Distribution of MgO and CaO contents is relatively low and complex between the rims and the cores (Figure 7). Only garnet from the border zone show homogeneous composition with no zoning. The compositional maps of Al, Mn, Fe, Ca and Mg distribution in garnet grain from intermediate zone (Figure 8) support zoning feature with enrichment of Mn in rim of the grains relative to the core. Thus, the profiles exhibited relatively Mn-poor central zones and relatively Mn-rich marginal rims, constituting a "spessartine inverse bell-shaped profile" (Figure 8).

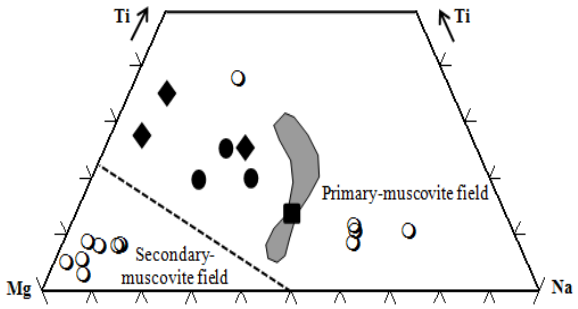

Fig.5. Composition of white mica in the studied garnet-bearing pegmatites on triangle diagram Mg-Ti-Na. The limit between fields for second and primary micas is from Miller et al. (1981). Grey field is representative white micas compositions in corderite bearing granitoids of Sierra de Chepes (Dahlquist et al., 2005). Field rhombuses are representative magmatic muscovite in garnet- bearing granitoids (Kebede et al., 2001). Filled of solid squares are representative magmatic muscovite in garnet-bearing granitoids of Piñón Rosado (Dahlquist et al., 2007).

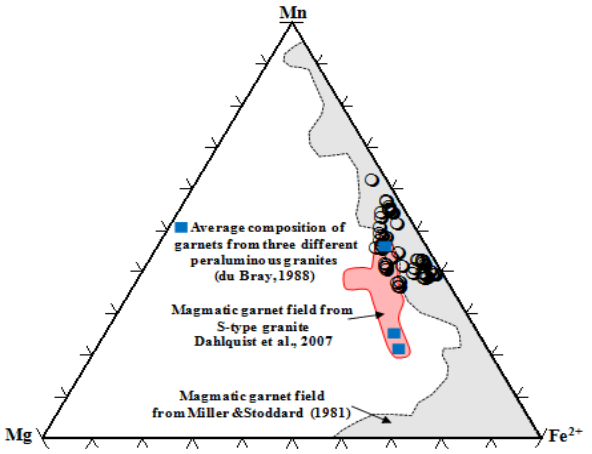

Fig.6. Garnet composition (Mn,Fe, and Mg) for the studied pegmatites compared with the magmatic garnet fields from Miller & Stoddard (1981) and Dahlquist et al., 2007.

Table 4. Representative major oxides for the garnet minerals from different pegmatite zones in Abu Had area, South Eastern Desert, Egypt.

Mineral Type	Garnet Core zone								Average 23 samples	Garnet Intermediate zone							Average 14 samples	Garnet Wall zone			Average 6 samples	Garnet Border zone				Average 9 samples
SiO2	36.80	37.00	35.54	37.00	37.05	35.57	35.40	35.25	36.30	36.30	36.45	36.30	36.80	35.80	35.40	36.15	36.90	36.72	36.60	36.74	35.70	36.15	35.70	36.55	36.06
TiO2	0.05	0.05	0.09	0.02	0.01	0.05	0.03	0.02	0.04	0.04	0.03	0.01	0.00	0.04	0.06	0.02	0.00	0.00	0.09	0.02	0.12	0.00	0.11	0.00	0.09
Al2O3	20.16	20.00	20.37	20.42	20.50	20.52	20.60	20.86	20.33	21.78	21.50	21.20	21.55	21.70	21.00	21.40	20.50	20.20	20.11	20.24	19.71	19.90	20.10	20.50	20.15
Cr2O3	0.04	0.00	0.00	0.00	0.00	0.03	0.00	0.01	0.01	0.00	0.00	0.00	0.00	0.00	0.00	0.00	0.00	0.00	0.00	0.00	0.00	0.00	0.00	0.00	0.00
FeO	21.03	20.90	20.56	20.35	19.38	19.81	18.40	17.50	20.38	21.51	19.34	19.75	18.30	18.40	16.50	19.51	18.61	16.70	14.20	17.39	18.12	18.51	19.10	19.60	18.66
MnO	13.70	14.83	15.98	16.22	17.02	17.62	19.45	20.50	15.51	14.57	16.13	16.80	18.00	18.80	21.50	16.97	18.81	21.00	24.60	20.36	25.13	24.16	23.55	22.04	23.84
MgO	0.37	1.27	0.70	1.54	1.80	1.43	1.53	1.63	0.86	2.33	2.35	2.29	2.05	2.39	1.16	2.18	2.00	1.25	0.69	1.61	0.65	0.63	0.72	0.76	0.69
CaO	7.85	5.78	7.00	4.60	4.15	5.23	4.13	3.80	6.46	3.64	4.38	3.72	3.10	3.00	4.02	3.77	3.14	4.17	3.60	3.62	0.45	0.43	0.52	0.61	0.45
Na2O	0.11	0.07	0.15	0.03	0.06	0.02	0.18	0.07	0.11	0.01	0.06	0.06	0.07	0.09	0.07	0.05	0.00	0.07	0.07	0.04	0.27	0.25	0.10	0.00	0.10
K_2O	0.00	0.00	0.00	0.00	0.01	0.01	0.00	0.00	0.00	0.00	0.00	0.00	0.01	0.00	0.01	0.00	0.00	0.00	0.00	0.00	0.03	0.04	0.06	0.03	0.03
Total	100.11	99.90	100.39	100.19	99.97	100.31	99.72	99.64	100.00	100.18	100.25	100.13	99.88	100.22	99.72	100.07	99.96	100.11	99.96	100.01	100.18	100.07	99.96	100.09	100.07
Structural formula based on 12 oxygen atom																									
Si	2.99	3.01	2.91	3.00	3.00	2.91	2.91	2.90	2.96	2.93	2.94	2.94	2.97	2.90	2.91	2.93	2.99	2.99	3.00	2.99	2.96	2.99	2.96	3.00	2.98
Ti	0.00	0.00	0.01	0.00	0.00	0.00	0.00	0.00	0.00	0.00	0.00	0.00	0.00	0.00	0.00	0.00	0.00	0.00	0.01	0.00	0.01	0.00	0.01	0.00	0.01
Al	1.93	1.92	1.96	1.95	1.96	1.98	2.00	2.02	1.95	2.07	2.04	2.02	2.05	2.07	2.03	2.04	1.96	1.94	1.94	1.94	1.93	1.94	1.96	1.98	1.96
Cr	0.00	0.00	0.00	0.00	0.00	0.00	0.00	0.00	0.00	0.00	0.00	0.00	0.00	0.00	0.00	0.00	0.00	0.00	0.00	0.00	0.00	0.00	0.00	0.00	0.00
Fe	1.43	1.42	1.41	1.38	1.31	1.35	1.26	1.20	1.39	1.45	1.30	1.34	1.23	1.25	1.13	1.32	1.26	1.14	0.97	1.18	1.26	1.28	1.32	1.35	1.29
Mn	0.94	1.02	1.11	1.11	1.17	1.22	1.35	1.43	1.07	0.99	1.10	1.15	1.23	1.29	1.50	1.16	1.29	1.45	1.71	1.40	1.77	1.69	1.65	1.53	1.67
Mg	0.04	0.15	0.09	0.19	0.22	0.17	0.19	0.20	0.11	0.28	0.28	0.28	0.25	0.29	0.14	0.26	0.24	0.15	0.08	0.20	0.08	0.08	0.09	0.09	0.09
Ca	0.68	0.50	0.61	0.40	0.36	0.46	0.36	0.33	0.56	0.31	0.38	0.32	0.27	0.26	0.35	0.33	0.27	0.36	0.32	0.32	0.04	0.04	0.05	0.05	0.04
Na	0.02	0.01	0.02	0.01	0.01	0.00	0.03	0.01	0.02	0.00	0.01	0.01	0.01	0.01	0.01	0.01	0.00	0.01	0.01	0.01	0.04	0.04	0.02	0.00	0.02
K	0.00	0.00	0.00	0.00	0.00	0.00	0.00	0.00	0.00	0.00	0.00	0.00	0.00	0.00	0.00	0.00	0.00	0.00	0.00	0.00	0.00	0.00	0.01	0.00	0.00
Total	8.04	8.04	8.12	8.03	8.02	8.10	8.10	8.10	8.07	8.04	8.05	8.06	8.01	8.07	8.08	8.05	8.03	8.04	8.03	8.04	8.09	8.06	8.06	8.01	8.05
Mg+Fe+Mn+Ca	3.10	3.10	3.21	3.08	3.06	3.21	3.17	3.16	3.13	3.04	3.06	3.09	2.98	3.08	3.12	3.07	3.07	3.10	3.08	3.10	3.14	3.09	3.11	3.02	3.08
Pyrobe	1.45	4.96	2.67	6.04	7.10	5.45	5.91	6.31	3.36	9.22	9.22	8.95	8.27	9.35	4.54	8.54	7.88	4.89	2.73	6.30	2.56	2.51	2.86	3.07	2.77
Almandine	46.10	45.85	43.78	44.81	42.93	42.23	39.90	38.01	44.41	47.70	42.52	43.30	41.45	40.40	36.27	42.98	41.13	36.67	31.59	38.19	39.99	41.45	42.54	44.49	41.82
Spessartine	30.42	32.95	34.45	36.17	38.19	38.04	42.72	45.10	34.21	32.74	35.92	37.31	41.29	41.81	47.87	37.86	42.10	46.71	55.42	45.33	56.18	54.80	53.12	50.67	54.10
Grossular	22.04	16.24	19.10	12.98	11.78	14.28	11.47	10.57	18.01	10.33	12.34	10.45	8.99	8.44	11.32	10.62	8.89	11.73	10.26	10.18	1.27	1.23	1.48	1.77	1.30

5.3.1. Trace and rare earth element composition of garnet

Data of LA-ICP-MS trace element [ppm] of euhedral garnet euhedral samples from the intermediate zone of pegmatite (Table 5) show low to extremely low abundances of Cs (□0.0001-0.019 ppm), Ba (□0.0001-0.16 ppm), Ni (0.01-0.36 ppm), Cr (0.27-0.86 ppm), Co (0.14-3.33 ppm), V (0.49-2.28 ppm), Sr (0.25-0.86 ppm), Rb (0.69-2.01 ppm), Hf (0.06-0.854 ppm), Ta (Pb (0.035-0.103 ppm), Ta (0.061-5.634 ppm), Th (0.07- 6.88 ppm), La (0.003-0.035 ppm), Ce (0.029-0.265 ppm), Pr (0.02-0.096 ppm), Eu (0.243-0.0.786 ppm), Nd (0.302- 1.468 ppm), Sm (1.407-4.148 ppm), Zr (1.31- 11.72 ppm), and Nb (0.24-56.14 ppm). In addition, analyzed garnet contains moderate to high concentration of Tb (27.359-64.781 ppm), Gd (31.830-79.178 ppm), Lu (49.511-181.066 ppm), Tm (69.237-218.415 ppm), Ho (147.717- 3630235 ppm), Yb (445.240-

1499.281 ppm), Er (466.916-13210.043 ppm), Dy (491.678-1156.703 ppm), and Y (5722.741-13586.393 ppm).

Chondrite-normalized rare earth element (REE) patterns (Figure 9) show that Abu Had garnets are characterized by extremly enrichment of HREE over LREE (Yb_N/Ce_N=10974 to 69780) and pronounced negative Eu anomalies (mean Eu/Eu*=0.13). Figure 9 also shows some within-grain variation, with garnet rims containing slightly lower REE contents compared to cores and/or steeper HREE profiles. Similarly, Y contents are significantly higher in the garnet core than in the rim (Table 5).

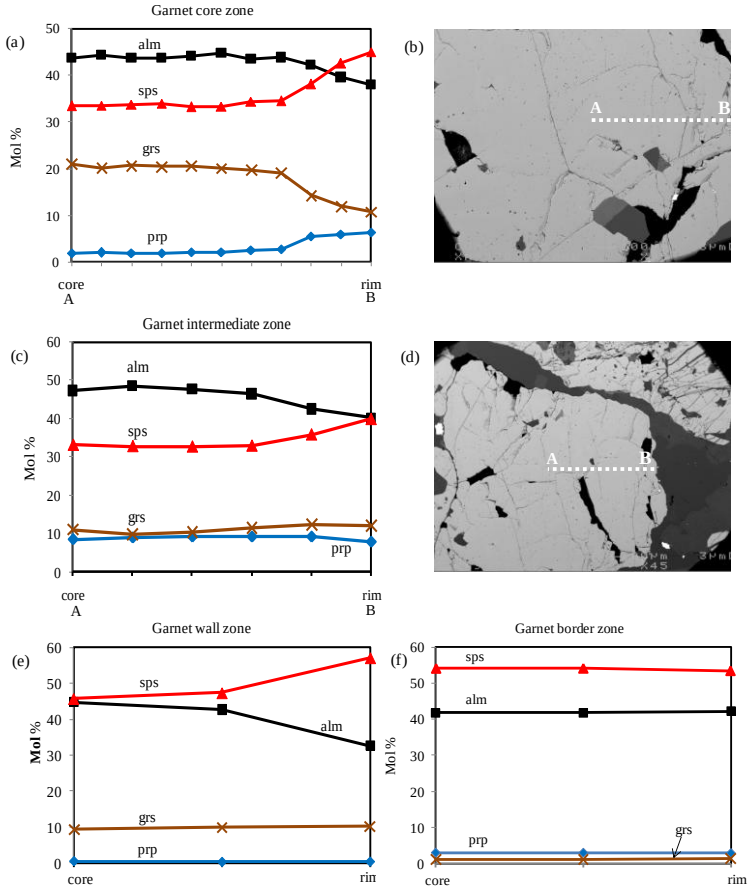

Figure 7. (a-b) electron-probe micro-analyzer line scan (A-B) and corresponding back-scattered images across garnet from the core zone. (c-d) electron-probe micro-analyzer line scan (A-B) and corresponding back-scattered image across garnet from the intermediate zone. (e) electron micro-analyzer line scan across garnet from wall zone. f) electron micro-analyzer linescan across garnet from border zone. Abbreviations: alm=almandine; sps=spessartine; grs=grossular; prp=pyrobe.

Table 6.Representative major oxides for the chlorite mineral from Abu Had pegmatite, South Eastern Desert, Egypt.

Element	Chlorite Core zone		Chlorite Intermediate zone		
SiO_2	26.42	26.30	27.96	27.90	29.00
TiO_2	0.06	1.80	0.00	0.17	0.16
Al_2O_3	20.10	20.00	21.10	19.00	19.80
Cr_2O_3	0.01	0.00	0.03	0.00	0.01
FeO	33.00	31.00	27.00	30.80	29.10
MnO	2.30	2.10	1.70	1.25	1.08
MgO	7.80	7.70	13.40	11.00	11.10
CaO	0.07	1.50	0.01	0.03	0.09
Na_2O	0.07	0.00	0.10	0.07	0.00
K_2O	0.08	0.09	0.01	0.18	0.04
Total	89.92	90.49	91.32	90.40	90.37
Structural formula based on 28 oxygen atom					
Si	5.70	5.60	5.70	5.87	6.01
Ti	0.01	0.29	0.00	0.03	0.02
Al	5.11	5.02	5.07	4.71	4.83
Cr	0.00	0.00	0.00	0.00	0.00
Fe	5.95	5.52	4.60	5.42	5.04
Mn	0.42	0.38	0.29	0.22	0.19
Mg	2.51	2.44	4.07	3.45	3.43
Ca	0.02	0.34	0.00	0.01	0.02
Na	0.03	0.00	0.04	0.03	0.00
K	0.02	0.02	0.00	0.05	0.01
Ni	0.00	0.00	0.00	0.00	0.00
Total	19.76	19.61	19.79	19.78	19.55
Fe/(Fe+Mg)	0.70	0.69	0.53	0.61	0.60

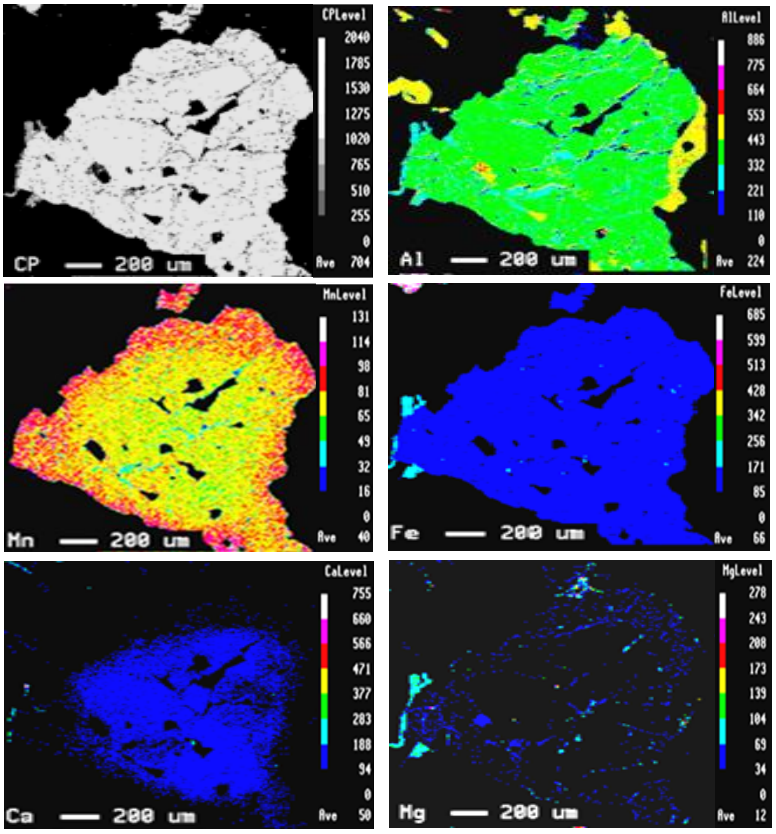

Figure 8. X-ray composition maps for Al, Mn, Fe, Ca, and Mg in the garnet of the intermediate zone from Abu Had pegmatite.

Table 5. LA-ICP-MS trace-element (PPM) of garnet from Abu Had pegmatite.

	Garnet						
	Rim						Core
Elements	1	2	3	4	5	6	7
Sc	162.1	119.4	104.1	116.9	164.4	334.5	273.1
Ti	185.0	413.7	499.5	355.5	952.1	629.2	905.1
V	0.64	0.49	0.55	0.66	0.72	2.28	1.39
Cr	0.27	0.40	0.46	0.62	0.59	0.41	0.86
Co	0.17	0.15	0.37	0.50	0.14	3.33	0.65
Ni	0.06	0.03	0.16	0.22	0.36	0.25	0.01
Ga	38.76	33.86	37.89	37.34	36.52	71.50	64.44
Rb	0.86	0.71	0.69	0.79	1.04	1.93	2.01
Sr	0.32	0.27	0.25	0.33	0.46	0.76	0.86
Y	6,426.005	5,720.983	5,722.741	5,762.031	6,997.187	11,220.981	13,586.393
Zr	1.31	4.65	3.83	1.96	11.72	2.38	9.94
Nb	0.24	13.71	4.69	2.52	27.52	30.58	56.14
Cs	0.003	0.001	0.001	0.002	0.001	0.019	□0.001
Ba	0.016	0.011	0.006	0.008	□0.001	□0.001	0.013
Hf	0.060	0.364	0.261	0.169	0.672	0.161	0.854
Ta	0.061	1.726	1.056	0.723	2.461	5.634	5.225
Pb	0.055	0.035	0.038	0.075	0.041	0.090	0.103
Th	0.070	0.894	0.128	0.059	6.880	0.143	0.274
La	0.003	0.007	0.001	0.007	0.034	0.013	0.035
Ce	0.032	0.078	0.029	0.048	0.265	0.069	0.197
Pr	0.032	0.039	0.020	0.032	0.079	0.055	0.094
Nd	0.509	0.348	0.302	0.675	0.588	1.246	1.468
Sm	1.633	1.407	1.440	1.527	1.956	4.148	3.520
Eu	0.243	0.413	0.394	0.258	0.501	0.314	0.786
Gd	36.824	36.461	35.478	31.830	42.480	56.710	79.178
Tb	31.904	29.700	29.068	27.359	33.740	49.493	64.781
Dy	561.127	506.344	500.149	491.678	592.889	926.362	1,156.703
Ho	165.617	149.558	147.717	154.550	183.434	301.937	363.235
Er	535.164	469.159	466.916	513.194	665.170	1,073.178	1,321.043
Tm	82.194	69.237	69.381	80.321	109.723	179.383	218.415
Yb	539.657	446.587	445.240	532.172	752.671	1,244.021	1,499.281
Lu	61.794	49.511	50.357	62.963	93.685	152.464	181.066
$(La/Sm)_N$	0.0011	0.0032	0.0006	0.0027	0.0110	0.0020	0.0062
$(La/Yb)_N$	0.000004	0.000011	0.000002	0.000008	0.000031	0.000007	0.000016
Eu/Eu*	0.10	0.17	0.17	0.11	0.17	0.06	0.14

5.4. Chlorite

Chlorite occurs as a secondary mineral within garnet cracks or associated with garnet rim in the microshear zones in the intermediate and core zone (Fig.4f). Composition data of chlorite are listed in Table 6. According to the chlorite classification diagram of Hey (1954), the studied chlorite has a composition between brunsvigite- pycnochlorite (Figure 10). This means that the chlorite is Fe-rich type revealing probably secondary derivation from garnet.

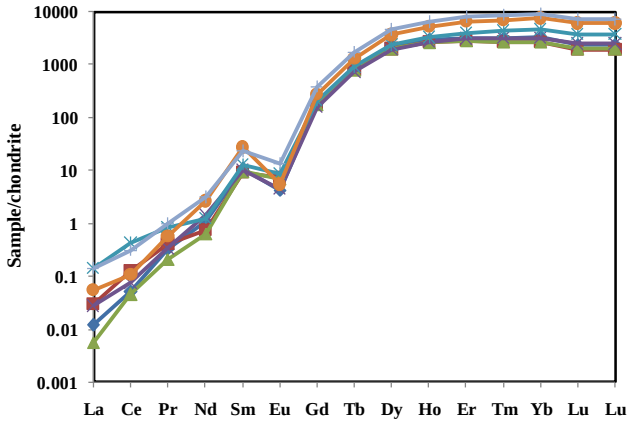

Figure 9. Chondrite-normalized rare earth element (REE) patterns of garnet from the intermediate zone of Abu Had pegmatite.

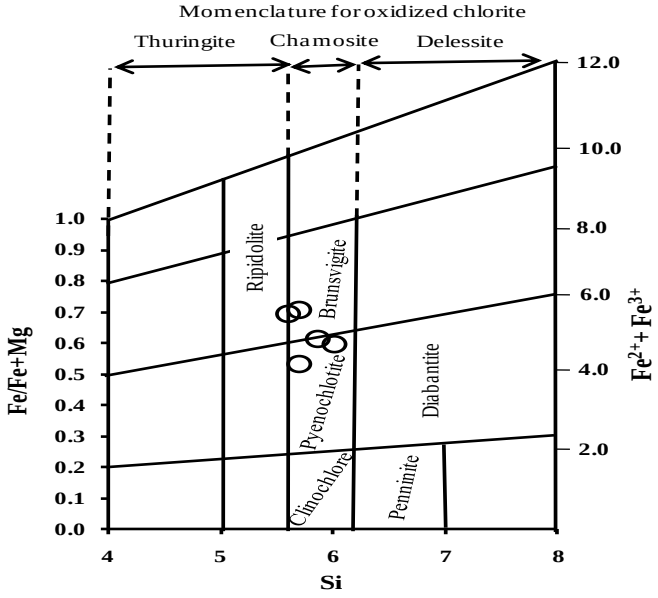

Figure 10. Nomenclature of chlorites and oxidized chlorites (Hey, 1954).

6. Whole rock chemistry

The results of chemical analyses of the studied granitoids country rocks are listed in Table 7. The gneissose tonalite-granodiorite have slightly lower SiO_2 contents compared to the leucogranites (68.85–71.40 wt% vs. 73.36–75.30 wt%). Following the R1-R2 classification scheme (Figure 11a) of Batchelor and Bowden (1985), the gneissose granites occupy the granodiorite and tonalite fields, while the leucogranites straddle the fields of monzo- to syenogranites. Clark (1992) used A/CNK vs. SiO_2 to discriminate between peraluminous and metaluminous granites as well as S- and I-type granites. The studied leucogranite samples are mainly peraluminous due to increasing A/CNK ratios [mol $Al_2O_3/(CaO + Na_2O + K_2O)$] >1 and plot mainly in the S-type granite field, while the gneissose tonalite-granodiorite plot in the I-type granite field and mainly have metaluminous characters (Figure 11b). Compared to Egyptian granitoids, using the Na–K–Ca ternary diagram (Figure 11c) designed by Hassan and Hashad (1990), the gneissose granodiorite-tonalite plot within the field of trondhjemitic older granitoids and generally follow the trondhjemitic trend of Barker and Arth (1976). The leucogranites plot along the Na_2O-K_2O line with some samples plot outside the field designated for the Egyptian younger granites.

The leucogranite show Rb and Th enrichments (relative to Nb), and Ce enrichment (relative to Nb and Hf), suggest crustal involvement (Pearce et al., 1984).

The REE patterns of the tonalite-granodiorite (Figure 12a) have LREE predominance over HREE (La/Yb= 3.21-6.60) and moderately negative to slightly positive Eu anomaly (Eu/Eu*= 0.60-1.13). The positive Eu anomaly for the tonalite sample and the negative Eu anomaly for the studied granodiorite, reflect that the latter formed through fractional crystallization for the former.

REE patterns of selected samples of the leucogranites (Figure 12b) are homogeneous, moderate to highly fractionated (La/Yb= 9.13-18.85; Table 7) and show marked negative anomaly (Eu/Eu*= 0.48-0.63). It comparable with the REE pattern of the Hafafit metasediments of Moghazi *et al.*, 2004 and also similar to REE pattern of the average upper continental crust (Taylor and McLennan, 1985).

Table 7. Chemical analyses of granitoids country rocks from Abu Had area, South Eastern Desert, Egypt.

	Lecogranite					Gneissose tonalite-granodiorite						
Sample	S1	S3	S6	S7	S10	G1	G2	G3	G4	G5	G6	G7
SiO_2	74.33	74.1	73.8	73.36	75.3	69.88	69.7	71.40	68.85	70.65	69.1	70.1
TiO_2	0.29	0.3	0.26	0.26	0.13	0.35	0.44	0.48	0.24	0.30	0.37	0.32
Al_2O_3	14.09	14.4	14.26	14.6	14.01	14.25	15.5	14.50	16.8	13.95	13.7	14.15
$Fe_2O_3^*$	1.37	1.03	0.9	1.2	1.09	3.55	2.2	3.40	1.7	3.30	4.2	3.63
MnO	0.03	0.05	0.04	0.04	0.03	0.08	0.03	0.06	0.04	0.07	0.08	0.08
MgO	0.38	0.28	0.3	0.4	0.36	1.68	1.06	1.10	0.72	1.58	2.7	1.57
CaO	0.75	0.76	0.8	0.88	1.14	3.63	3.1	3.60	4.3	3.54	3.3	3.7
Na_2O	3.77	3.5	3.38	4.33	3.88	4.12	5.4	3.80	5.4	4.36	3.97	4.1
K_2O	4.55	5.22	5.4	3.44	3.4	1.40	1.28	1.01	1.1	1.27	0.92	1.39
P_2O_5	0.2	0.19	0.16	0.24	0.12	0.08	0.08	0.08	0.06	0.08	0.09	0.08
L.O.I.	0.77	0.61	0.6	0.8	0.49	0.55	0.45	0.49	0.66	0.63	0.72	0.56
Total	100.51	100.44	100.45	99.55	99.88	99.6	99.24	99.9	99.87	99.7	99.15	99.68
A/CNK	1.14	1.13	1.03	1.18	1.16	0.95	0.96	1.04	0.82	0.94	0.98	0.93
Mg#	0.19	0.22	0.19	0.22	0.27	0.27	0.22	0.29	0.26	0.28	0.21	0.29
Trace elements (ppm)												
Rb	300	355	160	280	170	44	44	38	26	40	30	43.8
Ba	244	300	525	500	440	218	240	201	251	236	118.2	218
Pb	28	36	17	33	22	5	8	11	5	7	3.1	4.6
Sr	80	88	200	160	73	272	330	240	345	285	318	272
Y	17	14	19	11	34	8	13	11	12	8	14.6	8.1
Th	10	13	12	11	14	1	4	1	9	2	2.9	3
U	4	8	2	6	4	2	2	nd	3	1	1.7	2
Zr	100	90	138	126	144	79	135	120	103	62	95	72.3
Hf	3	4	6	5	8	4	3.3	8	2.8	2	3.2	3.7
Nb	13	14	6	12	9	4	1	6	1	2	1.4	1
Zn	44	40	33	50	45	45	31	33	23	30	66.7	45.4
V	12	9	8	13	11	56	25	40	18	48	58.9	55.6
Ga	21	25	18	23	20	16	18	12	22.3	14	15.9	15.9
REE (ppm)												
La	22.1	16.8		28.9		8.1		28			7.6	
Ce	44.00	39.20		66.10		21.8		55			19.20	
Pr	5.20	4.31		6.85		2.13		10			2.20	
Nd	19.0	16.5		23.8		9.3		27			8.0	
Sm	4.55	3.99		4.21		2		5			2.00	
Eu	0.65	0.79		0.57		0.4		1.26			0.68	
Gd	3.78	3.65		2.53		1.64		5			1.70	
Tb	0.68	0.61		0.49		0.19		1			0.30	
Dy	3.15	3.26		2.48		1.27		3.5			2.01	
Ho	0.53	0.52		0.44		0.26		0.65			0.47	
Er	1.41	1.44		1.22		0.74		1.85			1.43	
Tm	0.23	0.19		0.21		0.1		5			0.26	
Yb	1.28	1.32		1.10		0.88		3			1.70	
Lu	0.21	0.24		0.17		0.12		0.45			0.28	
La/Yb	12.38	9.13		18.85		6.60		6.42			3.21	
La/Sm	3.14	2.72		4.43		2.61		2.29			2.45	
Eu*	0.48	0.63		0.53		0.68		0.60			1.13	

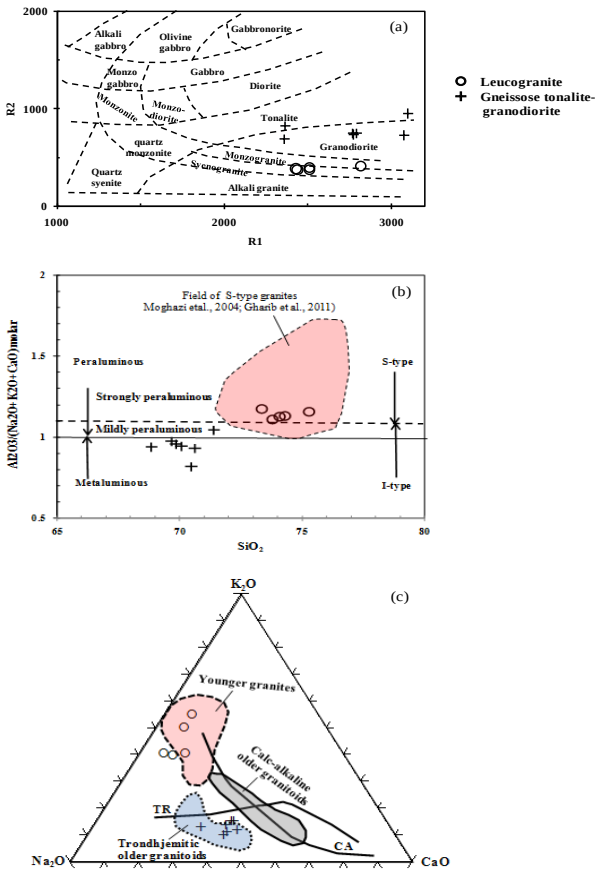

Figure 11. Geochemical classifications and discrimination diagrams for granitoid rocks of Abu Had area: (a) R1–R2 cationic classification of De la Roche et al. (1980). (b) A/CNK vs. SiO_2 diagram (Yuhara et al., (2003). (c) Na2O–K2O–CaO ternary diagram showing fields of the Egyptian granitoids (Hassan and Hashad, 1990). The trondhjemitic (TR) and calc-alkaline (CA) trends are from Barker and Arth (1976). R1= 4Si-11(Na+K)-(Fe+Ti), R2= 6Ca+2Mg+Al.

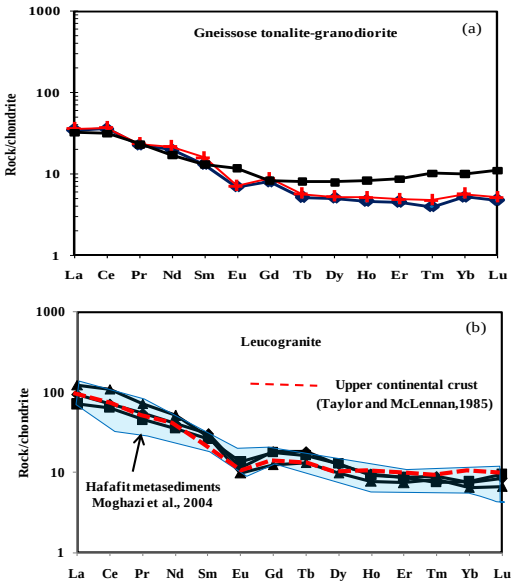

Figure 12. Chondrite-normalized REE plots for the studied granitoids (Sun&McDonough, 1989). (a) tonalite- granodiorite rocks (b) leucogranites compared to the Hafafit metsediments (Moghazi *et al.,* 2004) and upper continental crust (Taylor and McLennan, 1985).

7. Discussion

7.1. Tectonic settings of the granitoid rocks

Batchelor and Bowden (1985) suggested a diagram to discriminate between the different tectonic setting of granitic rocks using the multicationic parameters R1 and R2 of De La Roche *et al.* (1980). On this diagram (Figure 13a) the majority of gneissose tonalite- granodiorite plots in the pre-collision granite (subduction regime), while leucogranite samples plot in syn-collision granite regime. The studied leucogranites also plot within the field of S-type granites (Wise *et al.,* 2010; Gharib *et al.,* 2011). Following the delineated tectonic setting fields of Maniar and Piccoli (1989) on Figure 13b, the gneissose tonalite-granodiorite samples lie in the island arc granitoid field, while the leucogranite plot in the continental collision granite field. In the standard discrimination diagram of Pearce *et al.* (1984), the investigated gneissose tonalite- granodiorite have volcanic-arc (I-type) characters (Figure 13c), while the leocogranites straddle the fields of syn-collision and the volcanic arc fields and lie within the field of S-type granites (Wise *et al.,* 2010; Gharib *et al.,* 2011).

7.2. Origin of Gneissose tonalite- granodiorite

The Egyptian Eastern Desert granitoids could be intruded during the pre-, syn- and late-collisional stages of the East African Orogeny (Moghazi, 2002). He (op.cit.) stressed that the multi-element abundance spiderdiagrams are proved to be an effective means for discriminating the tectonic setting of the Egyptian granitoid rocks, especially the calc-alkaline (I-type) ones. The pre-collision granitoids in the Eastern Desert of Egypt are represented by highly deformed trondhjemite-tonalite-granodiorite suites and were formed during the arc stage of the Arabian Nubian Shield between 800 and 614Ma (Dixon, 1979; Stern and Hedge, 1985; Hassan and Hashad, 1990; Greiling *et al.,* 1994).

The chondrite-normalized spiderdiagrams (Figure 14a) of the investigated gneissose tonalite- granodiorite are more akin comparable with the field of pre-collision granites of the Eastern Desert (Moghazi, 2002) and confirmed with the tectonic setting data (Figures 13a and c).

Compositional differences of granitic melts produced by partial melting of various source rocks under variable melting conditions can be distinguished in terms K_2O vs. SiO_2 (Gerdes *et al.,* 2000). For the studied gneissic tonalite- granodiorite rocks, these major element ratios (Figure 15a) indicate that these rocks could be derived from partial melting of amphibolites source. The amphibolites source also proved from plotting the gneissic tonalite- granodiorite on the compositional fields of experimental melts derived from melting of felsic pelites (muscovite schists), metagreywackes and amphibolites (Patiño Douce, 1999) (Figures 15b, c and d). The slightly Y enriched patterns of the chondrite-normalized spiderdiagrams generally observed in the gneissose granitoids (Figure 14a) proved an amphibole-bearing, garnet-free, source. In addition, the negative Nb and Ti anomalies can also be explained by the presence of hornblende in the source. This support that gneissose tonalite-granodiorite wasderived by partial melting of a slightly LILE-enriched, garnet-free and amphibole-bearing (i.e., hydrated) mafic source. The experimental data obtained by Rapp and Watson (1995) on dehydration melting of metabasalts are in agreement with this hypothesis

.

7.3. Origin of Leucogranite

S-type granites are strongly peraluminous granitoids (ASI>1) result from the partial melting of aluminous metasediments (Chappell, 1984; Chappell and White, 1992; Chappell, 1999; Collins and Hobbs, 2001; Clemens, 2003; Dahlquist *et al.,* 2007; Burda *et al.,* 2009). Partial melting of metasedimentary composition is always produced leucogranite with FeO+MgO contents below 4 wt.% (e.g. Montel and Vielzeuf, 1997). Some authors believed that S-type granite to be the products of incongruent fluid-absent melting of biotite in aluminous sources (Le Breton and Thompson, 1988; Clemens, 1992; Vielzeuf and Montel, 1994; Patino-Douce and Beard, 1995; Montel and Vielzeuf, 1997). Experimental data from previous studies on the fluid-absent melting of metapelites (Vielzeuf and Montel 1994; Patino-Douce and Beard 1996) have demonstrated that the melts produced via the

anatexis of metapelites and metagreywackes are limited to leucocratic granitic compositions, particularly if it is considered that temperatures within the metamorphic crust only rarely exceed 900^{o}C (Harley, 1998).

The studied leucogranite are strongly peraluminous (ASI >1), K-rich granites with a substantial range in total FeO +MgO values (between 1.11 and 1.61 wt%) and have low Mg# range between 0.19-0.27 (Table 7). The presence of garnet, muscovite beside the high peraluminous nature in the studied leucogranite confirms the inference of an aluminous metasedimentary source. The low content of Fe and Mg in the leucogranite probably shows that the anatectic temperatures were mostly below the biotite solidus or that the source rocks themselves had a low content of biotite. Plotting the leucogranite on the Normative Qz–Ab-Or ternary diagram (Fig.16) proved moderate to low pressure of formation for these rocks which ranges between 1-10kbar in anhydrous system, and to the right of the cotectic eutectic minima of the H_2O saturated haplogranite system,

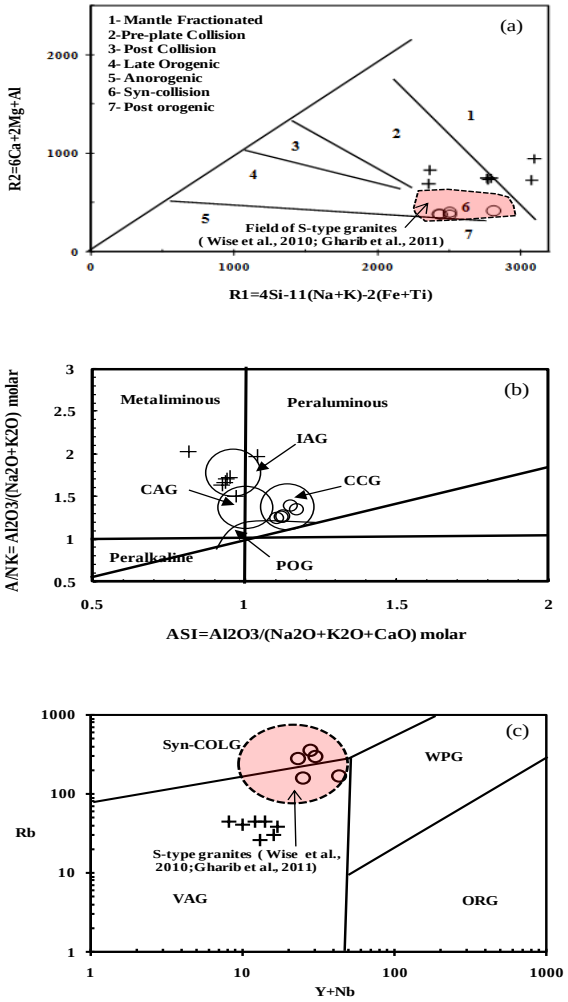

Figure 13. Tectonic setting discrimination diagrams for the studied granitoids: a) R1–R2 (Batchelor and Bowden , 1985). b) $Al_2O_3/Na_2O + K_2O$ vs. $Al_2O_3/Na_2O + K_2O + CaO$ diagram. Fields labeled IAG, CAG, CCG, and POG represent island arc granites, continental arc granites, continental collision granites and post-collision granites, respectively (Maniar and Piccoli, 1989). (c) Rb vs Y+Nb tectonic discrimination diagram of Pearce *et al.* (1984). Fields: Syn-COLG = syn-collision granites; VAG = volcanic-arc granites; WPG = within-plate granites and ORG = oceanic ridge granites.

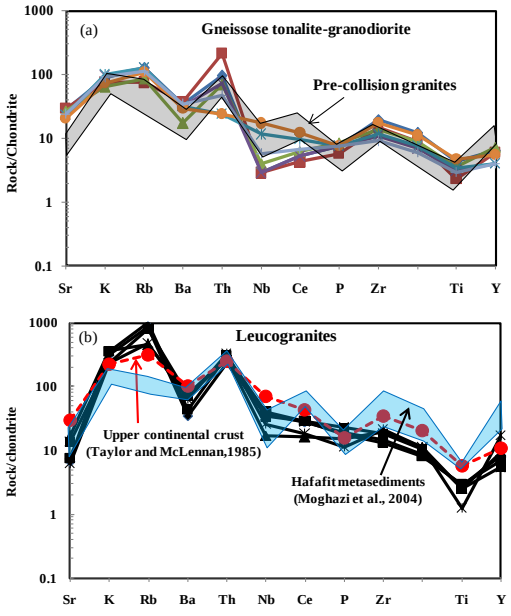

Figure 14. Chondrite-normalized spiderdiagrams for the studied granitoids.

a common feature for low temperature granites (Johannes and Holtz, 1996; Kalsbeek *et al.*, 2001; Moghazi *et al.*, 2004). The partial melting of metagreywake and metapellite source rocks is also proved by plotting the studied leucogranites on the fields of experimental melts derived from partial melting of different sources Figures 15a,b,c and d). Comparing the chondrite-normalized spiderdiagrams of the studied leucogranite with spiderdiagrams of Hafafit metasediments and the average of upper continental crust of Taylor and McLennan, 1984 (Figure 14b), shows enrichment of the leucogranites in K, Rb and depletion in Ba, Ce, Zr, Ti and Y suggest that the metasediment or the upper crust may be the source rock (Villaseca *et al.*, 2007).

According to Clemens, 1992; Clemens, 2003; Petford, 2003, the formation of high-level S-type granites can be summarized in four main stages; 1) Melting of a clastic metasedimentary source through a fluid-absent partial melting reaction, 2) The segregation of the magma from the residuum of its source, 3) The transport of the magma towards the future emplacement of granite, and 4) The crystallisation and emplacement of the granite. Accordingly, crustal thickening during the collision stage of the ANS led to a widespread partial- melting of a plagioclase-rich metasedimentary source (metagreywacke) and other associated crustal rocks. Crustal heating, caused by decompression along the NW- SE Wadi El Gemal major thrust or shear zones, facilate the source of heating and production of these leucogranitic melt. The melt then, at least partly, migrate along listric faults to higher levels in the crust due to pressure gradients generated by buoyancy and tectonic stresses (Nabelek *et al.*, 2001; Brown and Solar, 1998 a,b; Solar *et al.*, 1998, Moghazi *et al.*, 2004).

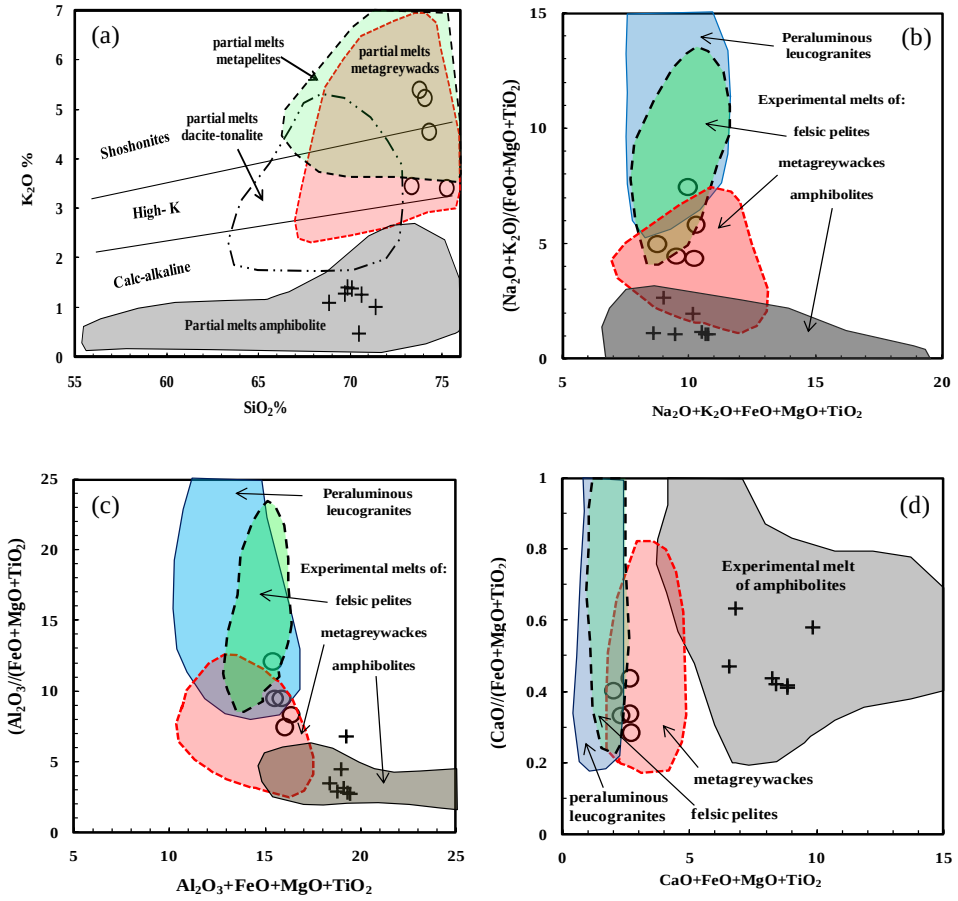

Figure 15. a) Discriminant diagrams for partial melts from various sources of Gerdes *et al.* (2000). (b, c and d) Compositional fields of experimental melts derived from melting of felsic pelites (muscovite schists), metagreywackes and amphibolites (Patiño Douce, 1999).

7.4. Origin of garnet

Garnet of Abu Had pegmatite have certain petrographical features like those of magmatic garnets which crystallize in granitoids, they tend to be eu- to subhedral, are commonly zoned and free or relatively free of inclusions, and are generally finely-crystalline (Allan and Clarke, 1981; Clemens and Wall, 1984; Wall *et al.*, 1987; Harrison, 1988; Speer and Becker, 1992; Macleod, 1992; Whitworth, 1992). Chemically, they are spessartine-almandine rich type and plotted in the field outlined by Miller & Stoddard (1981) for magmatic garnet (Figure 6), and in particular similar to garnet from peraluminous granitoids reported by du Bray, 1988 and Dahlquist *et al.*, 2007.

The compositional zoning of magmatic garnet is distinct from that of metamorphic garnet with high spessartine contents and typical spessartine-decreasing profiles from core to rim (Leake, 1967; du Bray, 1988). The crystallization of magmatic rocks takes place as temperature decreases, so that magmatic garnet generally display reversal zoning "spessartine inverse bell-shaped profile" with almandine-rich cores and spessartine-rich rims (Leake, 1967; du Bray, 1988; Dahlquist *et al.*, 2007; Villaros *et al.*, 2009). Consequently, the spessartine inverse bell-shaped profile for the studied garnets (Figures 7a-e and Figure 8) supporting their magmatic origin.

The strong enrichment of HREE over LREE, almost flat HREE patterns, profoundly negative Eu anomalies on the chondrite-normalized REE plots for the studied garnet (Figure 9), that are characteristic features of spessartine-rich garnet crystallized from silisic melts and of garnet in peraluminous granites and migmatites (Irving and Frey, 1978; Harris *et al.*, 1992; Bea *et al.*, 1994; Bea, 1996; Villaseca *et al.*, 2003). These REE patterns are also consistent with the REE patterns of magmatic garnet (Habler *et al.*, 2007; Jung *et al.*, 2009; Villaros *et al.*, 2009; Xia *et al.*, 2012). In contrast, negative Eu anomalies are not apparent

in metamorphic garnets formed by sub-solidus reactions (Harris *et al.*, 1992).

Magmatic garnet in igneous rocks can be classified into three groups: (1) it occurs in strongly peraluminous S-type dacites-rhyolites or granites and crystallized under low pressure in the upper crust with high FeO contents > 30 wt%) (Clemens and Wall, 1981, 1984; Gilbert and Rogers, 1989; Lackey *et al.*, 2006; René and Stelling, 2007; Mirnejad *et al.*, 2008); (2) occurs in basalts, andesites, dacites, rhyolites or tonalitic and granodioritic porphyries and crystallized under high pressure in the lower crust or mantle with FeO from 20-30 wt%, MgO from 5-10 wt%, and CaO about 5 wt% (Green and Ringwood, 1968; Hamer and Moyes, 1982; Day *et al.*, 1992; Harangi *et al.*, 2001; Aydar and Gourgaud, 2002; Patranabis-Deb *et al.*, 2009; Yuan *et al.*, 2009); and (3) occurs in pegmatites, aplites, and granites and crystallized from post-magmatic fluids or highly fractionated magma with MnO reach about 30 wt% (Speer and Becker, 1992; Whitworth, 1992). Thus, data of garnet of Abu Had pegmatite is conformable with magmatic origin crystallized from highly fractionated granites.

Igneous garnet with distinct chemical composition can crystallize from either an I, M, A and S type granites. Compositions of magmatic garnet from granites might provide information about the classification of their host (Zhang *et al.*, 2012 and references there in). Plotting the studied garnet on the diagram of magmatic garnet from various granite types (Figure 17), the Abu Had garnet is distributed mainly within the field of S-type granites confirming the peraluminous characters of the studied pegmatite which also attributed from the presence of abundant garnet and muscovite. Enrichment of many samples of Abu Had garnet in Mn contents relative to the S-granite type (Figure 16) probably related to more fractionated magma. The increase in Mn content could be not only related to magma cooling, but also to different hydration conditions (Robinson, 1991), which could be diverse in highly fractionated acid magmas. Thus, Enrichment of grossular contents in the studied garnet from the pegmatite core zone relative to the outer zones probably due to increasing H_2O in the magma (Green, 1992).

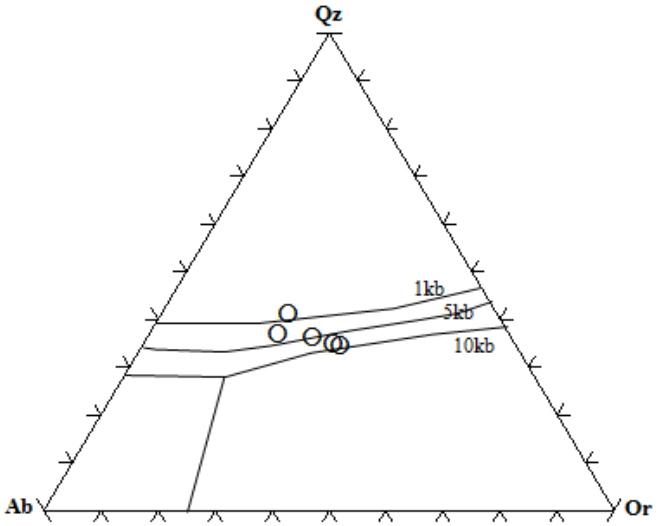

Figure 16. Plot the leucogranite in CIPW-normative Q–Ab–Or diagram with low temperature melt compositions at 1, 5 and 10 kb (Johannes and Holtz, 1996).

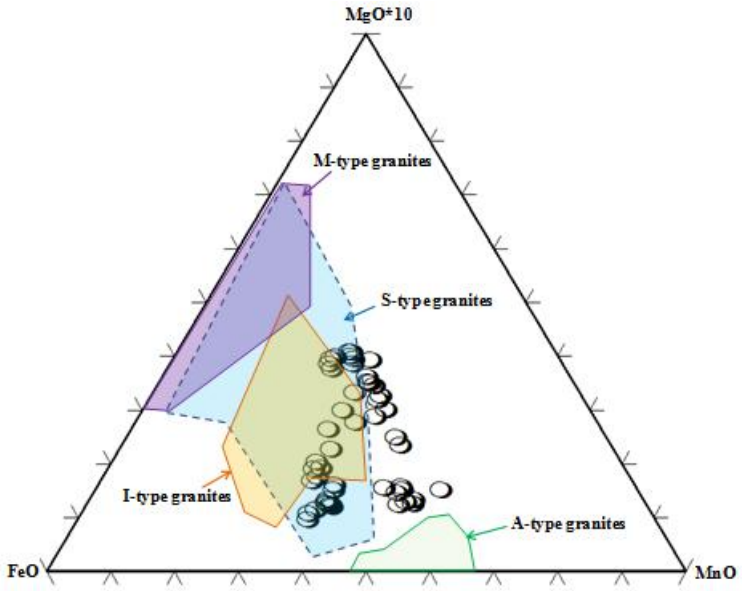

Figure 17. FeO-10 MgO-MnO triangular diagram of garnet from various genetic granites. I-type, S-type, A-type, and Mantle represent garnet from I-type granites, S-type granites, A-type granites, and igneous rocks originating from mantle. Major elements of garnet are from: I-type granites, Wu et al. (2004) and Yu et al. (2004); S-type granites, Plank (1987), Kebede *et al.* (2001), Jung *et al.* (2001), Jung and Hellebrand (2006), and Dahlquist *et al.* (2007); A-type granites, du Bray (1988), Wu *et al.* (2004), Wang *et al.* (2003), Zhang *et al.*, 2011; igneous rocks originating from mantle, Chen and Zhao (1991), Harangi *et al.* (2001), Kawabata and Takafuji (2005).

7.5. Petrogenesis of Abu Had pegmatites

Textural features of the studied garnet-bearing pegmatites such as micrographic intergrowth and absence of myrmekite, beside the data of mineral chemistry for the fresh rock-forming minerals support the magmatic origin for these pegmatites. Compositional data of garnet and muscovite from the Abu Had pegmatite proved peraluminous source rocks similar to those derived from the S-type granite magmas. As no samples from gneissic tonalite-granodiorite contain garnet beside the metaaluminous characters of these granitoids, it is difficult to link these rock types and the garnet bearing pegmatite through partial melting or fractional crystallization of garnet-bearing cumulates. The close spatial distribution of the pegmatites to the leucogranite bodies, textural and mineralogical similarity between the leucogranite and the neighboring pegmatites, beside the whole rock composition of the leucogranite probably indicate that these rocks are direct precursors to the garnet- bearing pegmatites of Abu Had area.

Spessartine-rich garnet generally crystallized in equilibrium with S-type, aluminum- and manganese-rich granitic magma at relative low pressures (Green, 1977; Abbott, 1981; Allan and Clarke, 1981; Stone, 1988; Dahlquist *et al.*, 2007). In contrast with those in S-type granitic plutons, garnet in metaluminous intrusions is characterized by Ca-rich, Mn-poor almandine and generally forms under relatively high pressure conditions, mostly corresponding to the depth of the crust-mantle transition zone (Day *et al.*, 1992; Green, 1992; Harangi *et al.*, 2001). Experimental studies of garnet stability (Weisbrod, 1974;Green, 1977; Clemens and Wall, 1981) have shown quite deafly that Mn-rich Fe-Mn garnets may be stable within a granitic melt at pressures below 5 kbar, and, with ever increasing Mn contents, may be stable at lower pressures (down to below 1kbar at 750^{o}C Weisbrod, 1974). Consequently, it is quite clear from experimental evidence that Mn rich garnets may crystallize directly from granitic magmas and pegmatitic liquids under conditions believed to obtain at a late magmatic stage. Miller and Stoddard (1981) stated that garnet could crystallize at the expense of biotite in MnO- and Al_2O_3-rich evolved magma. Many authors suggested that Mn-rich garnets crystallize from magmas enriched in volatile constituents (e.g. Baldwin and von Knorring, 1983; Bogoch *et al.*, 1997). Accordingly, the studied MnO-rich garnet relative to the typical S-type granite field (Zang *et al.*, 2011)(Figure 16), beside the complete absence of biotite in the studied pegmatites, support that the Abu Had garnet-bearing pegmatite crystallized from a highly evolved MnO-rich peraluminous magma. Consequently, Garent-bearing pergmatite of Abu Had area probably represent fractional crystallization for the same magma formed the associated leucogranites.

Field and petrographical observations indicate that the garnet-bearing pegmatite affected by post magmatic deformation and metasomatism which often restricted to the microshear zones and fracture sets associated with them. Growth of secondary muscovite or sericite along microcracks or cleavage planes, transformation of plagioclase to secondary albite and sericite and break down of garnet at the grains peripheries and along garnet fractures to chlorite and iron oxide, perhaps assisted by post magmatic aqueous fluid derived along active shear zones. Finally, pinch and swell of the pegmatite dyke (Figure 2a), beside cracking and stretching of some garnet crystals in direction perpendicular to the microshear zone (Figures 4g and h), prove that the study pegmatite and the associated country rocks exposed to extension tectonic event post-date the formation of garnet and the associated primary minerals.

7.6. Evolution of the study granitoids and pegmatites in relation to the regional tectonics of the ANS

Three geological stages were proposed for the tectonic evolution of the studied granitoids and garnet-bearing pegmatites. The first stage started at about 680 Ma (the estimated age for crystallization of the gneissose granite at Hafafit area; Stern and Hedge, 1985) with subduction and emplacement of subduction-related granitoids. This magmatism in the studied area is represented by the magma produced tonalite and granodiorite (precursor of the gneissose granites). Subduction was terminated by collision and NW-SE Wadi El Gemal thrusting. Geochemical data of the studied peraluminous leucogranites proved their formation during the collision stage of the ANS. These leucogranites were derived through partial melting of predominantly pelitic sources along thrust zones . Previous age dating studies indicate that the time of accretion or collision of ANS toward the Saharan Metacraton during the closure of Mozambique Ocean ranged between 620 and 600 Ma (Greilling *et al.*, 1994; Finger and Helmy, 1998; Cosca *et al.*, 1999; Fritz *et al.*, 2002). This geochronological data is in accordance with whole rock Rb–Sr ages for the peraluminous leucogranites from two different localities in Sikait area (about 20km north east of the studied area) which ranges between 610±20 and 594± 12Ma and interpreted as emplacement ages for these granites (Moghazi *et al.*, 2004). Crustal thickness during the collision of the ANS brings these metasediments and other associated crustal rocks in the study area close to their partial melting. Crustal heating, caused by decompression along the NW- SE Wadi El Gemal major thrust facilitate the source of heating and production of these granitic melt. Once generated, the leucogranite magma migrate along listric faults to shallower levels in the crust due to pressure gradients generated by buoyancy and tectonic stresses (Nabelek *et al.*, 2001; Brown and Solar, 1998 a,b; Moghazi *et al.*, 2004). Garent-bearing pegmatite of Abu Had area represents fractional crystallization for the same magma. At this stage, rocks of Hafafit unit including the study area were subjected to intense deformation and metamorphism in amphibolite facies which proved from the recorded Sm-Nb and Rb-Sr ages for this event (~600 Ma; Abd El-Naby *et al.*, 2008). Thus, generation of the leucogranite along thrust zones is related to this phase of metamorphism of Hafafit rocks. This interpretation is supported by the similarity between metamorphic age and granite emplacement age.

The third stage of evolution of the studied area is related to the late-orogenic extension and crustal thinning that was controlled by the Najd transform faults. Generally, the Najd fault system or shear zone regarded as the last significant structural event affected the Precambrian rocks in Egypt and Saudi Arabia (Stern 1985, 1994; Abd El-Wahed 2007, 2008, 2010; Abdeen *et al.*, 2008). It was developed during the interval 620-540 Ma (Stern, 1985). Fritz *et al.* (2002) reported the ages of 586 Ma for the NE extensional faults related to Najd fault system in WHC. The post magmatic deformation in the pegmatite and the leucogranite country rocks of the studied area with the abundant of microshear zones and related fractures probably related to this stage.

Corresponding author
Moustafa Esmail Gharib
Geology Department, Faculty of Science, Helwan University, Egypt
gharibme@yahoo.com

Acknowledgments
The authors are grateful to F. Finger, Salzburg University, Austria for microprobe analysis facilities. Deep thanks to S. Arai and A.H. Ahmed for their collaboration in laser ablation analysis at Kanazawa University, Japan

References

Abbott, R.N. Jr.,1981. AFM liquidus projections for granitic magmas, with special reference to hornblende, biotite and garnet. Canadian Mineralogist 19, 103-10.

Abd EL-Naby, H., Frisch,W., Siebel., W., 2008. Tectono-metamorphic evolution of the Wadi Hafafit Culmination (central Eastern Desert, Egypt). Implication for Neoproterozoic core complex exhumation in NE Africa. Geologica Acta 6, 293-312.

Abd El-Naby, H., Frisch, W., 2006. Geochemical constraints from the Hafafit Metamorphic Complex (HMC): evidence of Neoproterozoic back-arc basin development in the central Eastern Desert of Egypt. Journal of African Earth Science 45, 173-186.

Abd El-Naby, H., Frisch,W., 2002. Origin of Wadi Haimur-Abu Swayel gneiss belt, south Eastern Desert, Egypt: petrological and geochronological constraints. Precambrian. Research 113, 307-332.

Abd El-Naby, H., Frisch,W., Hegner, E., 2000. Evolution of Pan- African Wadi Haimur metamorphic sole, Eastern Desert, Egypt. Jounal of Metamorphic Geology 18, 639-651.

Abdelsalam, M.G., Stern, R.J., 1993. Structure of the late Proterozoic Suture, Sudan. Journal of Geological Society of London 150, 1065-1074.

Abdeen, M.M., Sadek, M.F., Greiling, R.O., 2008. Thrusting and multiple folding in the Neoproterozoic Pan-African basement of Wadi Hodein area, south Eastern Desert, Egypt. Journal of African Earth Science 52,21–29

Abd El-Wahed, M.A., 2007. Pan-African strike-slip tectonics of Wadi El-Dabbah area, north Sibai Core Complex, Central Eastern Desert, Egypt. Annals of the Egyptian Geological Survey 29, 1–36.

Abd El-Wahed, M.A., 2008. Thrusting and transpressional shearing in the Pan-African nappe southwest El-Sibai core complex, Central E. astern Desert, Egypt. Journal of African Earth Science 50, 16–36.

Abd El-Wahed, M.A., 2010. The role of the Najd Fault System in the tectonic evolution of the Hammamat molasse sediments, Eastern Desert, Egypt. Arab Journal of Geoscience 3,1–26

Allan, B.D., Clarke, D.B., 1981. Occurrences and origin of garnets in the South Mountain Batholith, Nova Scotia. Canadian Mineralogist 19, 19–24.

Aydar, E., Gourgaud, A., 2002. Garnet-bearing basalts: an example from Mt. Hasan, Central Anatolia, Turkey. Mineralogy and Petrology 75,185-201.

Barker, F., Arth, J.G., 1976. Generation of trondhjemite–tonalitic liquids and Archean bimodal trondhjemite–basalt suite. Geology 4, 596–600.

Batchelor R, Bowden, P., 1985. Petrogenetic interpretation of granitic rock series using multicationic parameters. Chemical Geology 48, 43–55.

Baldwin, J.R. and yon Knorring, O., 1983. Compositional range of Mn-gamet in zoned granitic pegmatites. Canadian Mineralogist 21,683-8.

Bea, F., 1996. Controls on the trace element composition of crustal melts. Trans. Royal Soc. Edinburgh-Earth Science 87,33-41.

Bea, F., Pereira, M.D. & Stroh, A., 1994. Mineral/leucosome traceelement partitioning in a peraluminous migmatite (a laser ablation-ICP-MS study). Chemical Geology 117, 291-312.

Bogoch, R., Bourne, J., Shirav, M. and Hamois L,.1997. Petrochemistry of a Late Precambrian garnetiferous granite, pegmatite and aplite, southern Israel. Mineralogical Magazine 61, 111-22.

Brown, M., Solar, G.S., 1998a. Shear-zone systems and melts: feedback relations and self-organization in orogenic belts. Journal of Structural Geology 20, 211–227.

Brown, M., Solar, G.S., 1998b. Granite ascent and emplacement during contractional deformation in convergent orogens. Journal of Structural Geology 20, 365–393.

Burda, J., Gawęda, A., 2009. Shear-influenced partial melting in the Western Tatra metamorphic complex: Geochemistry and geochronology. Lithos 110, 373–385.

Chappell, B.W. (1984) Source rocks of I- and S-type granites in the Lachlan Fold Belt, southeastern Australia. Philos Trans R Soc Lond A 310,693–707

Chappell, B.W., 1999. Aluminum saturation in I- and S-type granites and the characterization of fractionated haplogranites. Lithos 46, 535-551.

Chappell, B.W., White, A.J.R., 1974. Two contrasting granite types. Pacific Geology 8, 173-174.

Chappell B. W. and White A. J. R., 1992. I-Type and S-Type granites in the Lachlan Fold Belt. Trans. Royal Society of Edinburgh-Earth Science 83,1-26.

Chen, X.H., Zhao, Y.Q., 1991. Characteristics, genesis and petrogenic significance of garnet phenocrysts in acid lavas from the Xiling mining area. Geochimica 1, 33-39 (in Chinese with English abstract).

Clark, D.B., 1992. Granitoid Rocks. Chapman & Hall, New York, 283 p.

Clemens, J.D., 2003. S-type granitic magmas e petrogenetic issues, models and evidence. Earth-Science Reviews 61, 1-18.

Clemens, J. D., 1992. Partial melting and granulite genesis - a partisan overview. Precambian Research 55,297-301.

Clemens, J.D. and Wall, V.J., 1981. Origin and crystallization of some peraluminous (S-type) granitic magmas. Canadian Mineralogist 19, 111-31.

Clemens J.D. and Wall V.J., 1984. Origin and evolution of a peraluminous silicic ignimbrite suite: the Violet Town Volcanics. Contribution of Mineralogy and Petrology 88,354-371.

Collins, W.J., Hobbs, B.E., 2001. What caused the early Silurian change from mafic to silicic (S-type) magmatism in the eastern Lachlan Fold Belt? Austalian Journal of Earth Science 48, 25–41.

Cosca, M.A., Shimron, A., Caby, R., 1999. Late Precambrian metamorphism and cooling in the Arabian-Nubian Shield: Petrology and 40Ar/39Ar geochronology of metamorphic rocks ofthe Elat area (southern Israel). Precambian Research 98, 107-12.

Dahlquist, J.A., Galindo, C., Pankhurst, R.J., Rapela, C.W., Alasino, P.H., Saavedra, J., Fanning, C.M., 2007. Magmatic evolution of the Penon Rosado granite: petrogenesis of garnet-bearing granitoids. Lithos, 95: 177-207.

Dahlquist, J.A., Rapela, C.W., Baldo, E.G., 2005. Cordieritebearing S-Type granitoids in the Sierra de Chepes (Sierras Pampeanas): petrogenetic implications. Journal of South American Earth Science 20, 231–251.

Day, R.A., Green, T.H., Smith, I., 1992. The origin and significance of garnet phenocrysts and garnet-bearing xenoliths in Miocene calcalkaline volcanics from Northland, New-Zealand. Journal of Petrology 33, 125-161.

Deer, W.A., Howie, R.A., Zussman, J., 1992. An Introduction to the Rock Forming Minerals, Second Longman ed. Longman, London, 696 pp.

De la Roche, H., Leterrier, J., Grandcìaude, P., Marchal, M., 1980. A classification of volcanic and plutonic rocks using R1–R2 diagram and major element analyses – its relationships with current nomenclature. Chemical. Geology 29, 183–210.

Dixon, T.H., 1979. The evolution of continental crust in the Late Precambrian Egyptian Shield. Ph.D Thesis, California Univ., San Diego, 231 pp.

du Bray, E. A., 1988. Garnet compositions and their use as indicators of peraluminous granitoid petrogenesis-- southeastern Arabian Shield. Contribution to Mineralogy and Petrology100, 205-12.

El Gaby, S., List, F.K., Tehrani, R., 1988. Geology, evolution and metallogenesis of the Pan-African belt in Egypt. In: El Gaby, S., Greiling, R.O. (Eds.), The Pan-African Belt of NE Africa and adjoining Areas. Vieweg, Braunschweig, pp. 289–316.

El Ramly, M. F., Greiling, R., Kröner, A., Rashwan, A. A., 1984. On the tectonic evolution of the Wadi Hafafit area and environs, Eastern Desert of Egypt. Journal of King Abdulaziz University, Earth Sciences, 6, 113-126.

El Ramly, M.F., Greiling, R.O., Rashwan, A.A., Rasmy, A.H., 1993. Explanatory note to accompany the geological and structural maps of Wadi Hafafit area, Eastern Desert of Egypt. Geological Survey of Egypt, Paper No. 68.

Finger, F., Helmy, H.M., 1998. Composition and total-Pb model ages of monazite from highgrade paragneisses in the Abu Swayel area, south Eastern Desert, Egypt. Mineralogy and Petrology 62, 269–289.

Fritz, H., Dallmeyer, R.D., Wallbrecher, E., Loizenbauer, J., Hoinkes, G., Neumayr, P., Khudeir, A.A., 2002. Neoproterozoic tectonothermal evolution of the central Eastern Desert of Egypt: a slow velocity tectonic process of core complex exhumation. Journal of African Earth Science 34, 137–155.

Gerdes, A., Worner, G., Henk, A., 2000. Post – collisional granite generation and HT – LP metamorphism by radiogenic heating: the Variscan South Bohemian Batholith [J]. Journal Geological Society of London 157, 577 - 587.

Gharib, M. E., Saleh, G. M., Attia, G. M., Abu Zeid, E, k., and Mahmoud, G. B., 2011. Mineralogical and geochemical studies on the leucogranites at Gabal El Magal El Harami area, South Eastern Desert, Egypt. Egyptian Journal of Geology 55, 247-266.

Gilbert, J.S., Rogers, N.W., 1989. The significance of garnet in the Permo-Carboniferous volcanic-rocks of the Pyrenees. Journal of the Geological Society 146, 477-490.

Green, T.H., 1977. Garnet in silicic liquids and its possible use as a P-T indicator. Contributions to Mineralogy and Petrology 65, 59-67.

Green, T.H., 1992. Experimental phase equilibrium studies of garnet-bearing I-type volcanics and highlevel intrusives from Northland, New Zealand. Trans. R . Soc. Edinburgh: Earth Science 83, 429-438.

Green, T.H., Ringwood, A.E., 1968. Origin of garnet phenocrysts in calcalkaline rocks. Contributions to Mineralogy and Petrology 18, 163-174.

Greiling, R. O., Abdeen, M. M., Dardir, A. A., El Akhal, H., El Ramly, M. F., Kamal El Din, G. M., Osman, A. F., Rashwan, A. A., Rice, A. H. N. and Sadek, M. F., 1994. A structural synthesis of the Proterozoic Arabian-Nubian Shield in Egypt. Geol. Rundschau83, 484-501.

Hamer, R.D., Moyes, A.B., 1982. Composition and origin of garnet from the Antarctic Peninsula volcanic group of Trinity Peninsula. Journal of the Geological Society 139, 713-720.

Habler, G., Thoni, M., Miller, C., 2007. Major and trace element chemistry and Sm–Nd age correlation of magmatic pegmatite garnet overprinted by eclogite-facies metamorphism. Chemical Geology 241, 4–22.

Harangi, S., Downes, H., Kosa, L., Szabo, C., Thirlwall, M.F., Mason, P.R.D., Mattey, D., 2001. Almandine garnet in calc-alkaline volcanic rocks of the Northern Pannonian Basin (Eastern-Central Europe): geochemistry, petrogenesis and geodynamic implications. Journal of Petrology 42, 1813-1843.

Harley, S.L., 1998. On the occurrence and characterisation of ultrahigh temperature (UHT) crustal metamorphism. In: What Controls Metamorphism and Metamorphic Reactions? Treloar P.J. and O'Brien P. (eds), Special Publication Geological Society of London,138:75-101.

Harris, N.B.W., Gravestock, P., Inger, S., 1992. Ion-microprobe determinations of trace-element concentrations in garnets from anatectic assemblages. Chemical Geology 100, 41–49.

Harrison, T.N., 1988. Magmatic garnets in the Cairngorn granite, Scotland. Mineralogical Magazine 52, 659-67.

Hassan, M.A., Hashad, A.H., 1990. Precambrian of Egypt. In: Said R (ed) The geology of Egypt. Balkema, Rotterdam, pp 201–245.

Hey, M.H., 1954. A new reviewo f the chloritesM. Ineralogica Magazine, 30,272-292.

Hogan, J.P., 1996. Insight from igneous reaction space: a holistic approach to granite crystallization. Transactions of the Royal Society of Edinburgh: Earth Sciences 87, 147-157.

Irving, A.J., Frey, F.A., 1978. Distribution of trace-elements between garnet megacrysts and host volcanic liquids of kimberlitic to rhyolitic composition. Geochim Cosmochim Acta 42:771–787. doi:10.1016/0016-7037(78)90092-3.

Ishida, Y., Morishita, T., Arai, S., Shirasaka, M., 2004. Simultaneous in-situ multi-element analysis of minerals on thin section using LA-ICP-MS. The Science Reports of Kanazawa University 48, 31-42.

Johannes, W., Holtz, F., 1996. Petrogenesis and experimental petrology of granitic rocks. Minerals and Rocks 22. Springer, Berlin Heidelberg New York Tokyo, 335 pp.

Jung, C., Jung, S., Nebel, O., Hellebrand, E., Masberg, P., Hoffer, E., 2009. Fluid-present melting of meta-igneous rocks and the generation of leucogranites—Constraints from garnet major- and trace element data, Lu–Hf whole rock-garnet ages and whole rock Nd–Sr–Hf–O isotope data. Lithos 111, 220–225.

Jung, S., Hellebrand, E., 2006. Trace element fractionation during high-grade metamorphism and crustal melting-constraints from ion microprobe data of metapelitic, migmatitic and igneous garnets and implications for Sm-Nd garnet chronology. Lithos 87, 193e213.

Jung, S., Mezger, K., Hoernes, S., 2001. Trace element and isotopic (Sr, Nd, Pb, O) arguments for a mid-crustal origin of Pan-African garnetbearing S-type granites from the Damara orogen (Namibia). Precambrian Research 110, 325e355.

Kalsbeek, F., Jepsen, H.F., Nutman, A.P., 2001. From source migmatites to plutons: tracking the origin of c. 435Ma S-type granites in the East Greenland Caledonian orogen. Lithos 57: 1–21.
Kawabata, H., Takafuji, N., 2005. Origin of garnet crystals in calc-alkaline volcanic rocks from the Setouchi volcanic belt, Japan. Mineralogical Magazine 69, 951e971.
Kebede, T., Koeberl, C., Koller, F., 2001. Magmatic evolution of the Suquii-Wagaa garnet-bearing two-mica granite,Wallagga area, western Ethiopia. Journal of African Earth Sciences 32, 193-221.
Kontak, D. J. & Corey, M.,1988. Metasomatic origin of spessartine rich garnet in the South Mountain Batholith, Nova Scotia. Canadian Mineralogist 26, 315-334.
Lackey, J.S., Valley, J.W., Hinke, H.J., 2006. Deciphering the source and contamination history of peraluminous magmas using italic type^{18}O of accessory minerals: examples from garnet-bearing plutons of the Sierra Nevada batholith. Contributions toMineralogy and Petrology 151, 20-44.
Leake, B.E., 1967. Zoned garnets from the Galway granite and its aplites. Earth Planetary Science Letter 3, 311–316.
Manning, D.A.C., 1983. Chemical variation in garnets from aplites and pegmatites, peninsular Thailand. Mineralogical Magazine 47, 353–358.
Le Breton, N. & Thompson, A. B., 1988. Fluid-absent (dehydration) melting of biotite in metapelites in the early stages of crustal anatexis. Contributions to Mineralogy and Petrology 99, 226-237.
Macleod, G., 1992. Zoned manganiferous garnets of magmatic origin from the Southern Uplands of Scotland. Mineralogical Magazine 56, 115-6.
Maniar, P.D., Piccoli, P.M., 1989. Tectonic discrimination of granitoids. Geological Society of America Bulletin 101: 635–643
Miller, C.F., Stoddard, E.F., 1981. The role of manganese in the paragenesis of magmatic garnet: an example from the Old Woman-Piute Range, California. Journal of Geology 89, 233e246.
Miller, C.F., Stoddard, E.F., Bradfish, L.J., Dollase, W.A., 1981. Composition of plutonic muscovite: genetic implications. Canadian Mineralogist 19, 25–34.
Mirnejad, H., Blourian, G.H., Kheirkhah, M., Akrami, M.A., Tutti, F., 2008. Garnet-bearing rhyolite from Deh-Salm area, Lut block, Eastern Iran: anatexis of deep crustal rocks. Mineralogy and Petrology 94, 259-269.
Moghazi, A.M. 2002. Petrology and geochemistry of Pan-African granitoids, Kab Amiri area, Egypt: implications for tectonomagmatic stages in the Nubian Shield evolution. Mineralogy and Petrology 75, 41–67.
Moghazi, A.M., Hassanen, M.A., Mohamed, F.H., Ali, S., 2004. Late Neoproterozoic strongly peraluminous leucogranites, South Eastern desert, Egypt: petrogenesis and geodynamic significance. Mineralogy and Petrology 81, 19-41.
Monier, G., Mergold-Daniel, J.,Labernardiére, H. (1984): Générations successives de muscovites et feldspaths potassiques dans leucogranite du massif de Millevaches (Massif Central francais).– Bulletin of Mineralogy 107, 55–68.
Montel, J. M., Vielzeuf D., 1997. Partial melting of metagreywackes .2. compositions of minerals and melts. Contribution to Mineralogy and Petrology 128,176-196.
Morishita, T., Ishida, Y., Arai, S., Shirasaka, M., 2005. Determination of multiple trace element compositions in thin (<30 μm) layers of NIST SRM 614 and 616 using laser ablation–inductively coupled plasma–mass spectrometry. Geostandards and Geoanalytical Research 29, 107-122.
Nabelek, P. I., Lin, M., Sirbescu, M., 2001. Thermo-rheological, shear-heating model for leucogranite generation, metamorphism and deformation during the Proterozoic Trans-Hudson orogeny, Black Hills, South Dakota. Tectonophysics, 342, 371-388.
Patiño Douce, A.E., 1999. What do experiments tell us about the relative contributions of crust and mantle to the origins of granitic magmas? In: Castro, A., Fernandez, C., Vigneresse, J.L. (Eds.), Understanding granites: intergrating new and classical techniques. Geological Society London, Special Publication 168, 55– 75.
Patino-Douce A.E., Beard, J.S. (1995) Dehydration-melting of biotite gneiss and quartz amphibolite from 3 to 15 Kbar. Journal of Petrology 36,707–738.
Patino- Douce, A.E., Beard, J.S., 1996. Effects of P, f(O2) and Mg/Fe ratios on dehydration melting of model metagreywackes. Journal of Petrology 37, 999–1024.
Patranabis-Deb, S., Schieber, J., Basu, A., 2009. Almandine garnet phenocrysts in a similar to 1 Ga rhyolitic tuff from central India. Geological Magazine 146, 133-143.
Pattison, D.R.M., Carmichael, D.M. and St.-Onge, M.R., 1982. Geothermometry and geobarometry applied to early Proterozoic "S-type" granitoid plutons, Wopmay Orogen, Northwest Territories, Canada. Contribution to Mineralogy and Petrology 79, 394-404.
Pearce, J.A., Harris, N.B.W., Tindle, A.G. 1984. Trace element discrimination diagrams for the tectonic interpretation of granitic rocks. Journal of Petrology 69, 33–47.
Pearce, N.J.G., Perkins, W.T., Westgate, J.A., Gorton, M.P., Jackson, S.E., Neal, C.R., Chenery, S.P., 1997. A compilation of new and published major and trace element data for NIST SRM 610 and NIST SRM 612 glass reference materials. Geostandards Newsletter 21, 115-144.
Petford N., 2003. Rheology of granitic magmas during ascent and emplacement. Annal Review Earth Planetary Science 31,399-427.
Plank, T., 1987. Magmatic garnets from the Cardigan pluton and the Acadian thermal event in southwest New-Hampshire. American Mineralogist 72, 681e688.
Rapp, R.P. and Watson, E.B. (1995): Dehydration melting of metabasalt at 8-32 kbar: implications for continental growth and crust-mantle recycling. Journal of Petrology 36, 891-931.
René, M., Stelling, J., 2007. Garnet-bearing granite from the Třebíč pluton, Bohemian massif (Czech Republic). Mineralogy and Petrology 91, 55-69.
Robinson, P., 1991. The eye of the petrographer, the mind of the petrologist. American Mineralogist 76, 1 78 1 - 1 8 1 0.
Solar, G.S., Pressley, R.A., Brown, M., Tucker, R.D., 1998. Granite ascent in convergent orogenic belts: testing a model. Geology 26, 711–714.
Speer, J.A., 1984. Micas in igneous rocks. In Mineralogical Society of America Reviews in Mineralogy, 13,299-356.
Speer, J.A., Becker, S.W., 1992. Evolution of magmatic and subsolidus AFM mineral assemblages in granitoid rocks e biotite, muscovite, and garnet in the Cuffytown Creek, pluton, South-Carolina. American Mineralogist 77, 821-833.
Stern, R.J., 1985. The Najd Fault System, Saudi Arabia and Egypt: a late Precambrian rift related transform system? Tectonics 4, 497–511
Stern, R.J., 1994. Arc assembly and continental collision in the Neoproterozoic East African Orogen: implications for the consolidation of Gondwanaland. Ann Rev Earth Planet Sci., 22: 319–351.
Stern, R. J. and Hedge, C. E., 1985. Geochronologic and isotopic constraints on late Precambrian crustal evolution in the Eastern Desert of Egypt. American Journal of Science 285, 97-127.
Stoeser, D.B., Camp, V.E., 1985. Pan-African microplate accretion of the Arabian Shield. Geological Society of America Bulletin, 96, 817-826.
Stone, M., 1988. The significance of almandine garnets in the Lundy and Dartmoor granites. Mineralogical Magazine 52, 651-658.
Sun, S. S., McDonough, W. F., 1989. Chemical and isotopic systematic of ocean basalts: implication for mantle composition and processes. In: Saunders AD, Norry MJ (eds) Magmatism in the Ocean Basins. Geological Society of London, 42, 313-345.
Taylor S.R. and McLennan, S.M., 1985. The Continental Crust: Its Composition and Evolution. Blackwell Scientific Pub.,Palo Alto, CA, New York. P. 324.
Thöni, M., Miller, C., 2004. Ordovician meta-pegmatite garnet (N–W Ötztal basement, Tyrol, Eastern Alps): preservation of magmatic garnet chemistry and Sm–Nd age during mylonitization. Chemical Geology 209, 1–26.
Vielzeuf D. and Montel J.-M., 1994. Partial melting of metagreywackes .1. fluid absent experiments and phase-relationships. Contribution to Mineralogy and Petrology 117,375-393.
Villaros, A., Stevens, G., Buick, I.S., 2009. Tracking S-type granite from source to emplacement: clues from garnet in the Cape granite suite. Lithos 112, 217e235.
Villaseca, C., Martin Romera, C., De la Rosa, J. & Barbero, L., 2003. Residence and redistribution of REE, Y, Zr, Th and U during granulite-facies metamorphism: behaviour of accessory and major phases in peraluminous granulites of central Spain. Chemical Geology 200, 293-323.
Villaseca C., Orejana D. and Paterson B. A., 2007. Zr LREE rich minerals in residual peraluminous granulites, another factor in the origin of low Zr LREE granitic melts? Lithos 96:375-386.
Wall, V.J., Clemens, J.D., Clarke, D.H., 1987. Models for granitoid evolution and source compositions. Journal of Geology 95, 731-49.
Wang, R.C., Hu, H., Zhang, A.C., Xu, S.J., Wang, D.Z., 2003. Yttrium zoning in garnet from the Xihuashan granitic complex and its petrological implications. Chinese Science Bulletin 48, 1611e1615.
Weisbrod, A., 1974. Bull. Soc. Fr. Mineral. Cristallography 97, 61 70.
White, A., Clemens, J.D., Holloway, J.R., Silver, L.T., Chappell, B.W., Wall, V.J., 1986. S-type granites and heir probable absence in southwestern North-America. Geology 14, 115-118.
Whitworth, M.P., 1992. Petrogenetic implications of garnets associated with lithium pegmatites from SE Ireland. Mineralogical Magazine 56, 75-83.
Whitworth, M.P., Feely, M., 1989. The geochemistry of selected pegmatites and their host granites from the Galway Granite, western Ireland. Irland Journal of Earth Science 10, 89-97
Wise,M.A., Brown,C.D., 2010. Mineral chemistry, petrology and geochemistry of the Sebago granite–pegmatite system, southern Maine, USA. Journal of Geosciences 55,3-26.
Wu, F.Y., Sun, D.Y., Jahn, B.M., Wilde, S., 2004. A Jurassic garnet-bearing granitic pluton from NE China showing tetrad REE patterns. Journal of Asian Earth Sciences 23, 731-744.
Xia, Q. X., Zheng,Y.F., Lu, X., Hu, Z., Xu. H., 2012. Formation of metamorphic and metamorphosed garnets in the low-T/UHP metagranite during continental collision in the Dabie orogen, Lithos (2012), doi:10.1016/j.lithos.2011.10.004
Yuan, C., Sun, M., Xiao, W.J., Wilde, S., Li, X.H., Liu, X.H., Long, X.P., Xia, X.P., Ye, K., Li, J.L., 2009. Garnet-bearing tonalitic porphyry from East Kunlun, northeast Tibetan Plateau: implications for adakite and magmas from the mash zone. International Journal of Earth Sciences 98, 1489-1510.
Yuhara, M., Miyazaki, T., and Kagami, H. 2003. Rb-Sr and K-Ar gheochemistry and petrogenesis of the Aji granite in the eastern Sanuki district, Ryoke Belt, South West Japan. J. Min. and Petr., 98, 19-30.
Yu, J.H., Zhao, L., Zhou, X., 2004. Mineralogical characteristics and origin of garnet-bearing I-type granitoids in southeastern Fujian province. Geological Journal of China Universities 10, 364-377 (in Chinese with English abstract).
Zhang.J., Changqian Ma,C., She, Z., 2012. An Early Cretaceous garnet-bearing metaluminous A-type granite intrusion in the East Qinling Orogen, central China: Petrological, mineralogical and geochemical constraints. Geoscience Frontiers, 1-12, doi:10.1016/j.gsf. 11.011.
Zhou, X., Yu, J.H., 2001. Geochemistry of the granitoids in Mesozoic metamorphic belt of coastal Fujian province. Geochimica 30, 282-292 (in Chinese with English abstract).